ATP burst is the dominant driver of antibiotic lethality in Mycobacteria

Tejan Lodhiya[1], Aseem Palande[1], Anjali Veeram[1], Gerald Larrouy-Maumus[2], Dany J V Beste[3], Raju Mukherjee[1, *]

[1]Department of Biology, Indian Institute of Science Education and Research (IISER), Tirupati, India

[2]Centre for Bacterial Resistance Biology, Department of Life Sciences, Faculty of Natural Sciences, Imperial College London, London, UK

[3]Department of Microbial Sciences, Faculty of Health and Medical Sciences, University of Surrey, Guildford, UK

*Corresponding author - raju.mukherjee@iisertirupati.ac.in

Running title: Bactericidal effect of ATP burst

Teaser: Cidal drugs kill mycobacteria by ATP intoxication from energy overcharge.

Abstract: Antibiotic-tolerant bacteria, due to their unique physiology, are refractory to antimicrobial killing and pose challenges for infection control. Incomplete knowledge of how bactericidal antibiotics work limits our understanding of partial resistance from phenotypic tolerance in mycobacteria, a driver for developing genetic resistance. Using proteomics, ^{13}C isotopomer analysis, and biochemical assays, we investigated the physiological response of *M.smegmatis* challenged with aminoglycoside and fluoroquinolone antibiotics. Two distinct classes of antibiotics elicited remarkably similar responses and increased flux through the TCA cycle, causing enhanced respiration, ROS generation, and ATP burst. We found that ATP burst drives cidality through metal ion chelation, which was rescued by exogenous supplementation with divalent metals. ^{13}C isotope tracing indicated TCA cycle flux deviation from its oxidative arm as a bacterial adaptive mechanism, which also included activated intrinsic resistance and a higher propensity to develop antibiotic resistance. Our study provides a new understanding of the intricate mechanisms of antibiotic-induced cell death and expands the current paradigm for antibiotic action.

Introduction: Antibiotics have saved millions of lives from bacterial infections, however, the emergence of resistance against all classes of antibiotics renders clinically available antibiotics ineffective and undermines efforts to combat lethal bacterial infection. Antimicrobial resistance (AMR) is responsible for approximately 7,00,000 deaths per year and, if left unchecked, is projected to exceed 10 million by 2050 (1). The conventional approach for combating AMR through pathogen-specific antibiotics is no longer viable, as the drug discovery pipeline has shrunk over the past several decades. Therefore, there is a pressing need to develop novel interventions for preserving and enhancing the efficacy of the existing drugs through synergy or adjuvant therapy. However, there are gaps in our understanding of how precisely the existing antibiotics mediate cell death and what are bacterial counter responses to these challenges at a system-wide scale.

Antibiotics are commonly believed to cause cell death either by inhibiting essential cellular processes facilitating cell division or compromising the integrity of the cell envelope, while antibiotic resistance involves more complex mechanisms and manifests as genotypic resistance, antibiotic tolerance, and persistence. Interestingly, Kohanski *et al.* proposed that regardless of the target, a shared mechanism of antibiotic action involves damage produced by reactive oxygen species (ROS)(2). Furthermore, respiration-decelerating antibiotics were found to inhibit the cidality of respiration-accelerating antibiotics(3), highlighting the requirement of an in-depth understanding of the drug's mode of action, in a combination therapy. While the deleterious effect of ROS on bacterial physiology is intuitive, at sub-lethal concentrations, ROS was found to promote multidrug resistance by triggering superoxide radical-induced mutations(4). These observations demonstrate that the mechanism of antibiotic lethality is more complex than previously understood. Therefore, it is pivotal to look beyond drug-target interactions and comprehend the numerous mechanisms by which antibiotics induce cell death. The bacterial counter responses to these mechanisms would result in the emergence of phenotypic and, eventually, genetic resistance.

Antibiotic tolerance results from physiological adaptation that enables a bacterial population to withstand lethal doses of antibiotics for a longer duration and also provides the driving force to develop genetic resistance(5). Although the significance of antibiotic tolerance is recognized, the precise metabolic state and sequence of the adaptive events leading to the development of antibiotic tolerance remain poorly characterized. *M. tuberculosis*, the etiological agent for tuberculosis, a prominent cause of death from infectious disease, shows

exceptional tolerance to antibiotics and partly explains the reason for a long treatment regimen requiring a combination of antibiotics(6). Despite having low rates of mutation and recombination, the rapid increase in multi- and extensively drug-resistant tuberculosis infections compels us to re-examine our current understanding of the mechanisms of antibiotic action in mycobacteria. A systemic investigation of the physiological responses to antibiotic exposure prior to the emergence of resistance holds the key to deciphering the nature and quantum of antibiotic induced stresses. In this study, we employed temporal quantitative proteomics and ^{13}C isotopomer analysis to comprehensively understand the physiological responses of the model organism, *M. smegmatis*, exposed to sub-lethal concentrations of antibiotics from two distinct classes, fluoroquinolone and aminoglycoside. Through genetic and biochemical assays we show the involvement of ROS and ATP burst in antibiotic lethality. Finally, we demonstrate metal ion chelation by ATP as a dominant factor driving cell death post ATP burst. Our findings contribute to a deeper understanding of the complex mechanisms underpinning antibiotic-induced cell death in mycobacterium with implications for preventing the development of antibiotic tolerance and resistance.

Results:

Exposure to sub-lethal doses of aminoglycoside and fluroquinolone reveals physiological adaptation without genetic resistance.

In order to understand the biology of antibiotic-stressed mycobacteria, we designed a growth assay to measure the responses of mycobacteria to sublethal antibiotic concentrations. *M. smegmatis mc²155* was challenged with either 1x, ½x, or ¼x MBC_{99} (minimum bactericidal concentration) of fluoroquinolone (norfloxacin) and aminoglycoside (streptomycin) antibiotics. While 1x MBC_{99} and ½x MBC_{99} concentrations were lethal and growth-inhibitory, respectively, growth at sub-lethal concentrations (i.e., ¼x MBC_{99}) of both antibiotics exhibited a prolonged lag phase **(Fig. 1A and 1B)**.

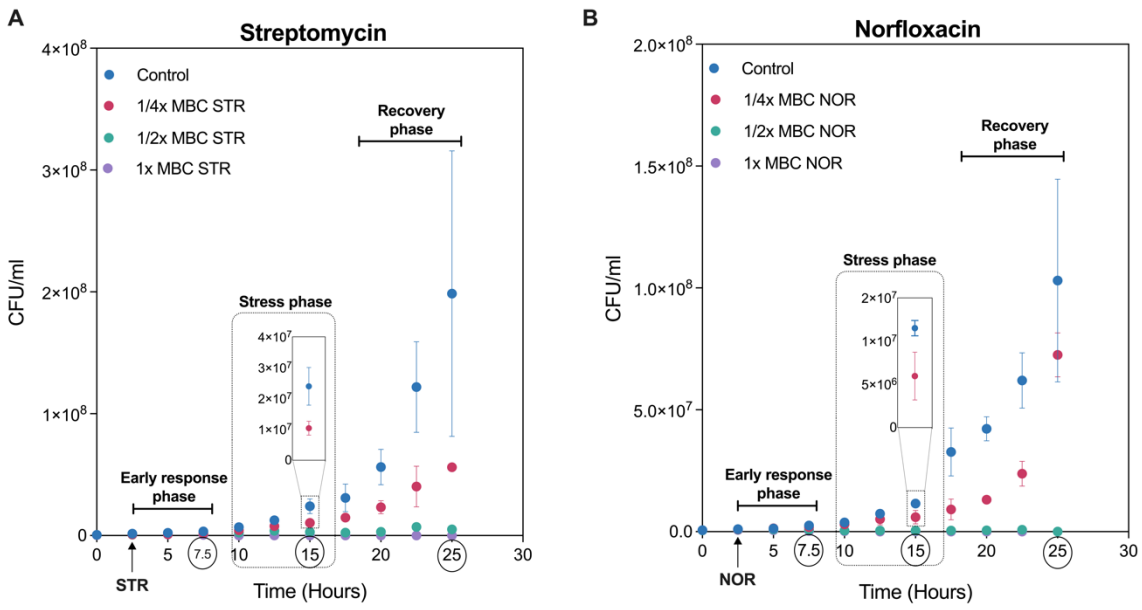

Fig. 1. Exposure to sub-lethal doses of aminoglycoside and fluroquinolone reveals physiological adaptation to antibiotics. The growth curve of *M. smegmatis* challenged with either 1x, ½x, or ¼x MBC_{99} of streptomycin (A) or with norfloxacin (B). Data points represent the mean of at least three independent replicates ± SD. 1x MBC_{99} of streptomycin (250 ng/ml) and 1x MBC_{99} of norfloxacin (2 µg/ml).

To decipher the antibiotic-induced growth changes, we divided the growth curve into three phases: an early response phase (5 hours post treatment), which is a period shortly after the addition of antibiotics, and showing no visible differences in the growth rate; a stress phase (5-17.5 hours post treatment), characterized by reduced growth rate and prolonged lag time; and a recovery phase (17.5-25 post treatment), in which mycobacterial growth rate resumes following antibiotic adaptation. The experiments were terminated when the culture reached stationary phase (~ OD = 1) to prevent the stationary phase response from interfering with the antibiotic induced response. The prolonged lag time observed during the stress phase is of profound significance in deciphering the nature of antibiotic-induced stresses and has implications for the development of antibiotic tolerance(7). Similarly, a thorough understanding of the recovery phase cells can reveal cellular determinants involved in adaptation to antibiotics. Towards this end, we first ruled out whether the resumption of growth on sub-lethal concentrations of antibiotics was due to the emergence of an antibiotic-resistant population. For this, bacteria were harvested from the recovery phase (25-hour), and the MIC of the antibiotics on cells grown with and without ¼x MBC_{99} of the same antibiotic were

compared. No changes in MIC confirmed that the growth resumption during the recovery phase was physiological rather than a result of genetic resistance **(S1A and S1B)**.

Norfloxacin and streptomycin have shared mechanism of action.

We performed untargeted label-free quantitative (LFQ) proteomics on mycobacteria grown with and without ¼x MBC_{99} of both antibiotics, during all three growth phases to observe the physiological alterations in mycobacterium exposed to antibiotics,. Six data sets yielded a total of 2,982 distinct proteins (43% of the *M. smegmatis* proteome), with each sample identifying roughly 2000 proteins **(S2A)** thus demonstrating the robustness of our methodology. To ascertain the reproducibility across samples, the data for each condition were subjected to rigorous quality control analysis **(S2B)**. Differentially expressed proteins were defined as those crossing a fold change threshold of ±2 and a p-value of ≤ 0.05. A volcano plot analysis revealed the differential expression of several proteins in response to both antibiotics **(Fig. 2A and 2B)**.

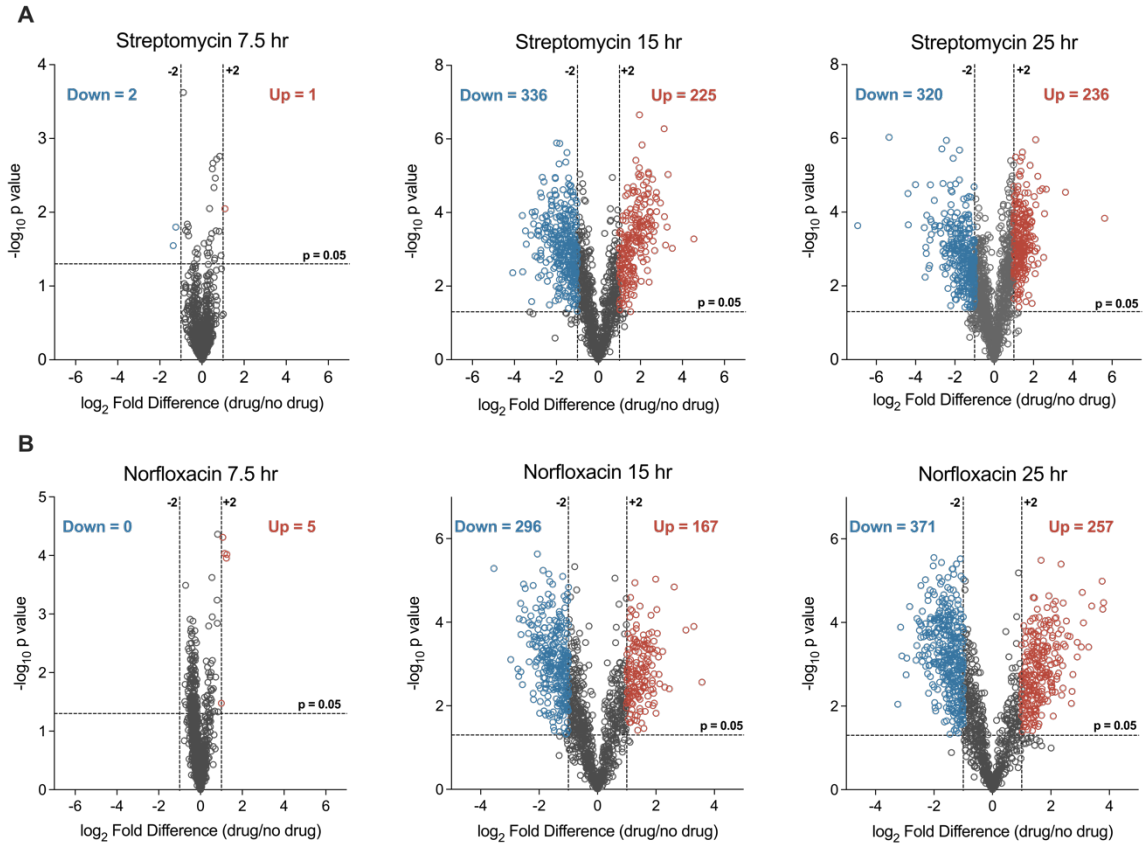

Fig. 2. Differential expression analysis of total proteome upon norfloxacin and streptomycin treatment. Volcano plot analysis of the proteins temporally quantified at 7.5 hr, 15 hr, and 25 hr time points for

streptomycin (A) norfloxacin treatment (B). Each dot represents one protein. Fold change cut off ±2 and a t-test significance cut-off of ≤ 0.05 were applied to identify differentially expressed proteins, shown in different colours.

Corresponding to the unaffected growth rate in the early response phase (7.5-hour), the proteomic profile of antibiotic-treated cells was indistinguishable from that of the control group at this time point. In contrast, cells from the stress phase (15-hour) and the recovery phase (25-hour) displayed several up- and down-regulated proteins in response to both antibiotics. We also noted a transition from a coordinated to an uncoordinated state of the proteome, and back to an unperturbed state depending on the time for growth recovery. Consistent with its mode of action, streptomycin (STR) treatment up-regulated proteases, peptidases, and proteasomal complex components implicated in the degradation of misfolded proteins **(Fig. 3A)**. Likewise, norfloxacin (NOR) treatment induced the SOS response by down-regulating LexA, the repressor of SOS response, and up-regulating DNA repair proteins such as RecA/B/C and PafC **(Fig. 3A)**. These data indicate that the sub-lethal doses of antibiotics used in our study exert sufficient stress on their primary targets. Next, we sought to determine the secondary consequences of antibiotic-target interactions. Towards this end, proteins involved in central dogma (DNA replication, transcription, and translation), and cell cycle and cell division processes were found significantly down-regulated in response to both the antibiotics **(Fig. 3B to 3D)**, correlating with the observed decrease in growth rate during the stress phase. Our results suggest that the initial bacterial response to antibiotics may involve downregulation of essential cellular processes that are required for optimal growth and antibiotic lethality.

To look for a shared mechanism of antibiotic action (2,8), we performed a Pearson correlation analysis between the NOR and STR induced alteration in proteome from the stress **(Fig. 3E)** and recovery phases **(S3A)**. The results revealed a highly correlated (Pearson coefficient (r) > 0.90) proteomic profile of antibiotic-treated mycobacteria in the stress phase **(Fig. 3E)**, indicating that structurally and functionally distinct antibiotics produce a strikingly similar response. To determine the cause of these similarities, we attempted to gain a deeper insight into the shared processes impacted by antibiotics. For this, we conducted pathway enrichment analysis on proteins that were up-regulated and exclusively expressed upon antibiotic treatments. As depicted in figure **S3B**, pathway enrichment analysis showed that central carbon metabolic pathways were enriched for both antibiotics. Notably, enzymes of the TCA cycle (CitA, Icd, Acn), glyoxylate shunt (Icl1 and GlcB), GABA shunt, the anaplerotic node (Pck, Pca), and PPP shunt (G6-PDH, 6-PGD) were significantly up-regulated for both

antibiotics, suggesting metabolic alterations in response to antibiotic treatment (**Fig. 3F and 3G**). Collectively, these data advocate for a common mechanism of antibiotic action that extends beyond their primary targets.

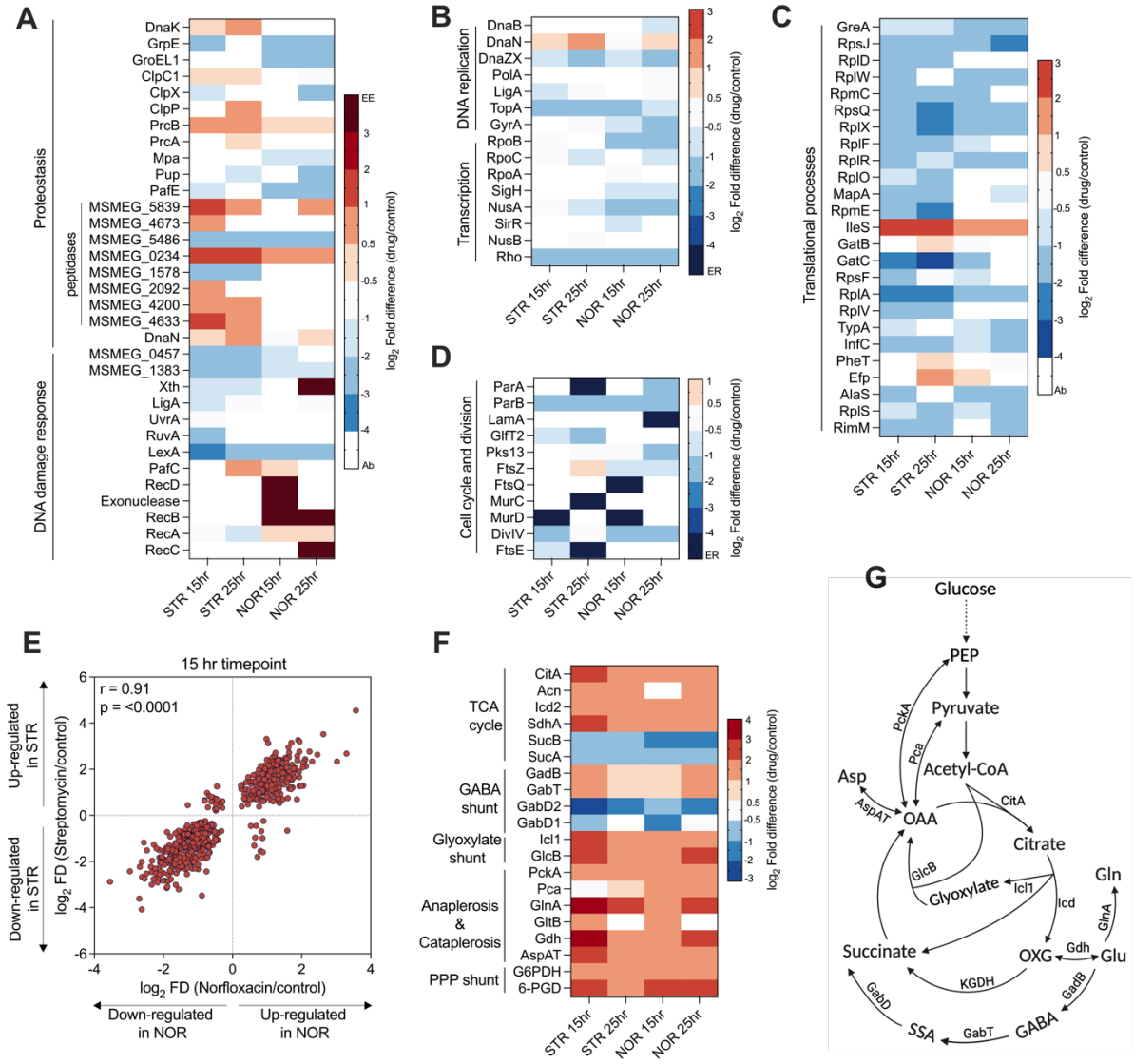

Fig. 3. Norfloxacin and streptomycin have common mechanism of action. Heat map analysis represents the $\log_2$ fold changes of proteins involved in (A) DNA damage response and proteostasis network, (B) DNA replication and transcription, (C) translation, and (D) cell cycle and cell division processes, identified from proteomics data. Colours in the heat map depicts the extent of differential expression, where EE demonstrates exclusively expressed, ER demonstrates exclusively repressed/absent in response to antibiotics, and Ab represents proteins that were not identified or quantified, with high significance. (E) Scatter plot of the Pearson correlation analysis of common proteins identified upon NOR and STR treatment. Each dot represents a single protein with its $\log_2$ fold difference for NOR (x-axis) and STR (y-axis) treatment at t = 15 hour time point. (F) Heat map

depicting the $\log_2$ fold changes of proteins involved in central carbon metabolism (CCM) of *M. smegmatis*. Figure (G) illustrates the CCM pathway of *M. smegmatis*.

Norfloxacin and streptomycin generate reactive oxygen species to confer cidality.

Studies have reported that reactive oxygen species (ROS) are generated as a secondary consequence of antibiotic-target interaction and facilitate cell death by oxidizing vital biomolecules(8). Therefore, we anticipated an antioxidant response upon antibiotic treatment due to ROS production. In agreement with this hypothesis, the antibiotic treated proteome revealed a significant upregulation of anti-oxidant enzymes such as catalases, superoxide dismutases, mycothione reductase, and methionine sulfoxide reductase (MsrA) (**Fig-4A)**. The upregulation of enzyme MsrA, involved in the repair of the oxidized proteins, indicates ROS mediated protein oxidation. In addition, anti-oxidant proteins such as alkylhydroxyperoxidase, bromoperoxidase, and peroxiredoxin were exclusively expressed in response to antibiotics, suggesting that bacteria may have experienced oxidative stress upon antibiotic treatment. Together, these data suggest that the treatment with NOR and STR induces ROS production.

In order to directly measure oxidative stress (due to intracellular ROS production) in response to antibiotics, we used the Mrx1-roGFP2 redox biosensor(9). It is a ratiometric fluorescence reporter that measures the intracellular redox potential of mycobacteria and has been extensively used to measure the redox state of cells *in-vitro* and *ex-vivo* (9–11). The sensor exhibits an increased fluorescence ratio at 405/488 nm excitation under oxidative stress, and a reduced ratio under reductive stress. The ability of the biosensor to measure oxidative and reductive stress was confirmed using an oxidizing and a reducing agent in comparison to the untreated control **(S4A)**, demonstrating its reliability in sensing oxidative stress in mycobacteria. Thereafter, to interrogate whether the antibiotics induce oxidative stress, we administered sub-lethal to lethal doses of both antibiotics to Mycobacteria containing the biosensor. Exposure to either NOR or STR increased the fluorescence ratio at 405/488 nm, suggesting generation of ROS in a time **(Fig. 4B and 4C)** and concentration-dependent manner **(Fig. 4D and 4G)**. Furthermore, antibiotic-induced ROS was directly detected using the CellROX deep red dye. A dose-dependent increase in the mean fluorescence intensity was observed in the case of NOR (**S4B)**, which however, was not significant upon STR treatment, presumably due to the selectivity of CellROX dye to detect superoxide ($O_2^{\bullet -}$) ions(12), whose levels may be lower in case of STR.

Next, we sought to investigate whether ROS contributed to antibiotic lethality. Towards this end, we first established whether glutathione (GSH) can quench antibiotic-induced ROS. Indeed, co-treatment with GSH prevented an increase in the 405/488 nm ratio upon antibiotic treatment **(S4C and S4D)**. To check the impact of ROS on cell survival, an antibiotic time-kill curve was performed with a supra-lethal dose (10x-MBC_{99}) of the antibiotics over a duration predetermined to result in the death of > 99.9% of cells(13), in the absence and presence of GSH. As observed in **Fig. 4E and 4H**, co-treatment with GSH substantially inhibited the lethality of antibiotics, demonstrating that antibiotic-induced ROS contributed to cell death.

ROS is known to damage nearly all macromolecules, including DNA, proteins, and lipids. Proteins of TCA cycle enzymes and the ETC chain incorporate Fe-S clusters for electron exchange that are very susceptible to ROS-induced damages, resulting in the release of iron (Fe^{+2}) in the cytoplasm. Free hydroxyl radicals are generated via the Fenton cycle, which results in further ROS production and could also contribute to antibiotic-induced cell death(14). Using the iron-chelator bipyridyl (BP), known to inhibit the Fenton cycle-mediated ROS burst, we found that indeed, iron sequestration significantly reduced antibiotic induced-death **(Fig. 4F and 4I)**. Collectively, the induction of the antioxidant response, the detection of ROS using the Mrx1-roGFP2 biosensor, and the mitigation of antibiotic lethality using glutathione and Fenton cycle inhibitor confirms that both NOR and STR treatment cause increased ROS production as a part of their lethality.

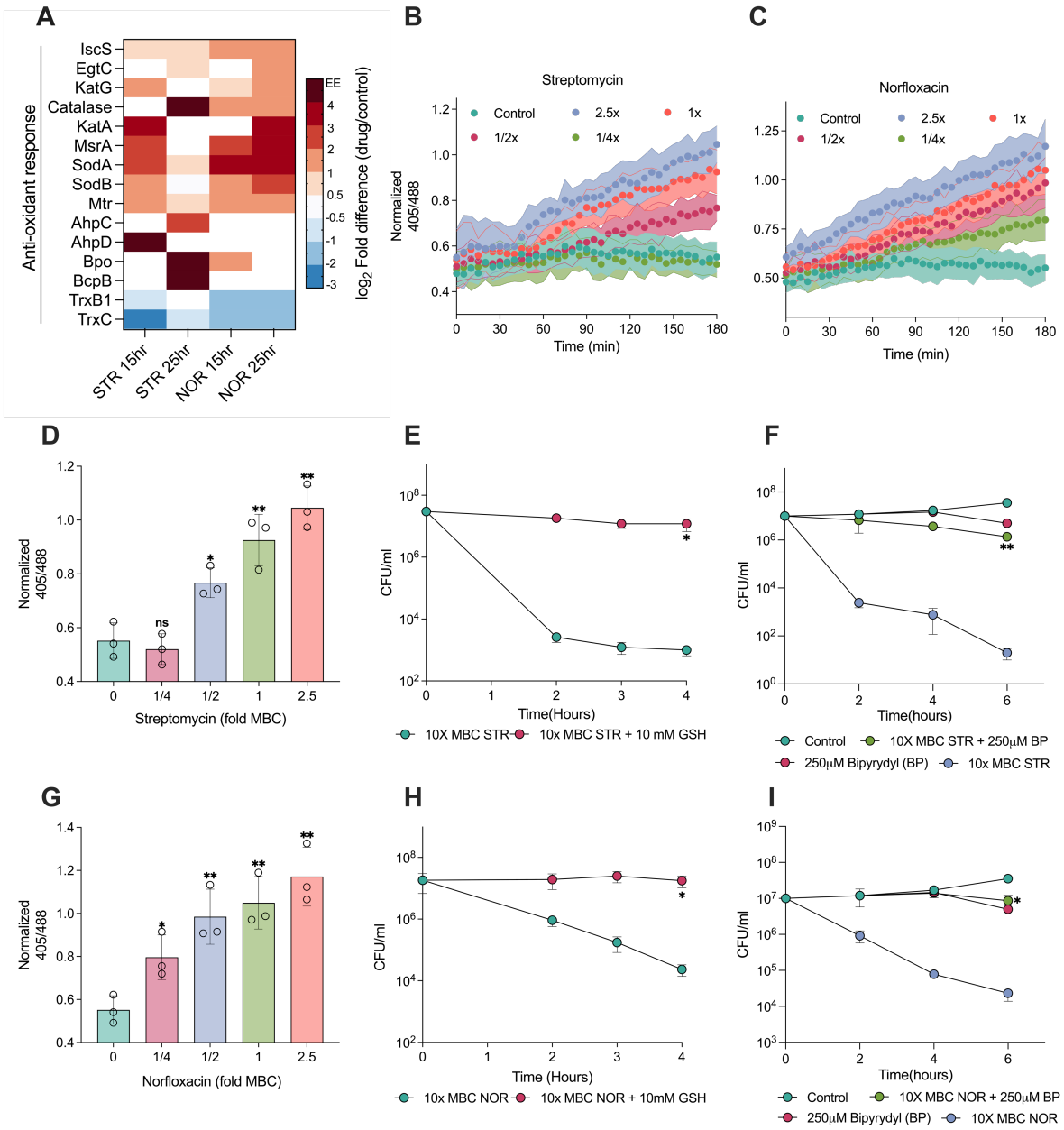

Fig. 4. Norfloxacin and streptomycin generate reactive oxygen species as part of their lethality. The heat map (A) depicts the $\log_2$ fold differences of proteins involved in antioxidant response. EE demonstrates proteins that are exclusively expressed in response to NOR or STR. Temporal (B and C) and dose-dependent (D and G) ratiometric response of *M. smegmatis* expressing Mrx1-roGFP2 redox biosensor upon STR and NOR treatment at 3 hour. The biosensor fluorescence measurements were recorded at the excitation of 405 nm and 488 nm, for a common emission at 520 nm. Figures demonstrate the effect of 10 mM glutathione on the survival of *M. smegmatis* treated with lethal dose (10x MBC_{99}) of STR (E) and NOR (H). Figures (F) and (I) presents the effect of bipyridyl on the survival of *M. smegmatis* treated with lethal dose of STR and NOR, respectively. Data

points represent the mean of at least three independent replicates ± SD. Statistical significance was calculated by students' t-test (unpaired), *$p < 0.05$, **$p < 0.01$, ***$p < 0.001$.

Norfloxacin and streptomycin treatment induces a burst in ATP levels.

Despite knowing the significance of ROS generation in bacterial physiology, our understanding of its origin, precise cause, and the stimulus, remains unclear. Since the electron transport chain (ETC) is the primary source of ROS production by electron leakage, we hypothesized that the increase in ROS levels resulted from enhanced respiration. To test this, we measured the levels of ATP, the end product of aerobic respiration, in response to antibiotics. Expectedly, NOR and STR treatments induced a time- and dose-dependent increase in ATP production, suggesting an increase in respiration (**Fig. 5A to 5F)**. Elevated ATP levels observed under antibiotic treatment were also confirmed using the mycobacteria specific ATP/ADP ratiometric biosensor, PHR-mCherry(15). Data presented in figure **S5A**, demonstrate a dose-dependent increase in ATP/ADP ratio upon NOR and STR treatments. To further confirm whether enhanced respiration caused elevated ATP levels, we employed the redox dye resazurin to measure bacterial respiratory activity upon antibiotic treatments, as reported earlier(16). Resazurin reduction assay showed enhanced fluorescence conversion rate in bacteria treated with antibiotics, thus confirming increased respiration rate **(S5B and S5C)**. Intriguingly, the observed rise in ATP levels upon antibiotic treatment was inversely proportional to cell survival **(Fig. 5A to 5F)**. Respiration rate has been linked to antibiotic action with accelerated respiration potentiating antibiotic lethality(17). Thus, our results suggest that antibiotic-treated cells exhibit a significant increase in respiration, resulting in an ATP burst that is associated with bacterial death.

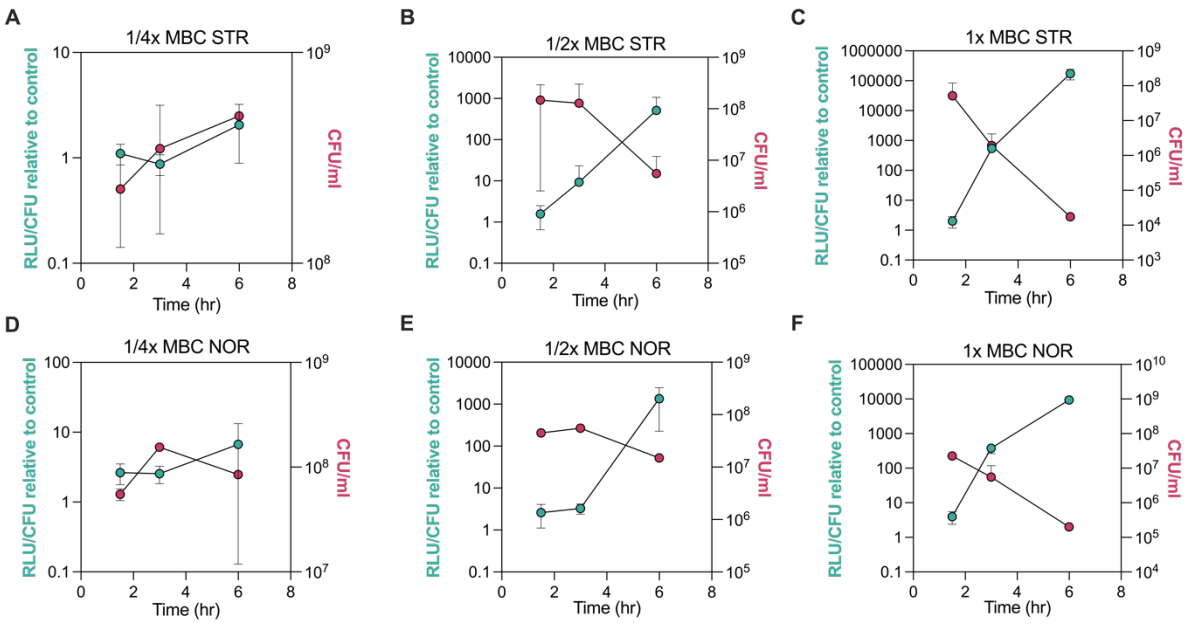

Fig. 5. Norfloxacin and Streptomycin treatment induces a lethal burst in ATP levels. Time-course of relative luminescence measurements representing ATP levels in *M. smegmatis* in response to ¼x (A & D), ½x (B & E) 1x MBC_{99} (C & F) of streptomycin & norfloxacin, respectively. The right y-axis represents the viability of cells measured just before the measurement of ATP. 1x MBC_{99} for STR and NOR are 1 µg/ml and 16 µg/ml, respectively. All data points represent the mean of at least three independent replicates ± SD.

Elevated ATP levels contributes to antibiotic cidality

We next sought to decipher whether the elevated ATP production was a consequence or a cause of antibiotic lethality. To establish the contribution of increased ATP levels to mycobacterial death, it was necessary to specifically inhibit the antibiotic-induced ATP burst without changing the metabolic rate. Towards this, we co-treated cells with antibiotics and carbonyl cyanide 3-chlorophenylhydrazone (CCCP), a protonophore, at non-toxic levels **(S5D to S5F)** to mitigate ATP burst. Protonophore uncouples oxidative phosphorylation from ETC, thus relieving the back-pressure on ETC and increasing respiration. Notably, co-treatment with CCCP dissipated the antibiotic-induced ATP burst in a dose-dependent manner (**Fig. 6A-B, 6D-E)**, confirming that the increase in ATP levels mediated by NOR and STR treatment was the result of increased respiration followed by oxidative phosphorylation. Subsequently, we reasoned that if ATP burst contributes directly to antibiotic action, then dissipating antibiotic-induced ATP burst would increase bacterial survival on antibiotics. To test this hypothesis, we compared antibiotic kill curves with CCCP (mitigating ATP burst) and without CCCP (causing ATP burst). As observed in **Figure 6C and F**, co-treatment with CCCP significantly inhibited

antibiotic-induced cell death, demonstrating the role of ATP burst in antibiotic lethality. This finding was further confirmed using the gene deletion mutant of one of the two copies of *atpD* gene, encoding the β subunit of the ATP synthase. The *M. smegmatis* Δ*atpD* single mutant has diminished levels of the β subunit, causing respiratory slowdown and lower ATP levels(18). Due to its energy compromised physiology, we anticipated that Δ*atpD* would be unable to generate an ATP burst at wild type scale, upon antibiotic treatment. Indeed, Δ*atpD* strain displayed lower ATP levels **(Fig. 6G)** and enhanced survival **(Fig. 6H to 6I)** upon antibiotic treatment, hinting at the significant contribution of ATP burst towards antibiotic lethality. To ascertain our finding, we used bedaquiline (BDQ), a known inhibitor of mycobacterial ATP synthase, to suppress antibiotic induced ATP burst. BDQ is known to have a delayed effect on *M. smegmatis* ATP levels, with 100x MIC of BDQ reducing cellular ATP levels by only 10 fold after 2 days of treatment(19). Therefore, we sought to give a pre-treatment of BDQ before challenging cells with NOR and STR. While 24 hours of pre-treatment with BDQ at 25x to 200x-MIC_{99} had no effect on cell survival, they significantly reduced the killing rate of STR **(Fig. 6J)** and NOR **(Fig. 6K)**. Together, we conclude that mitigation of antibiotic induced ATP burst using a chemical or genetic method reduces antibiotic lethality.

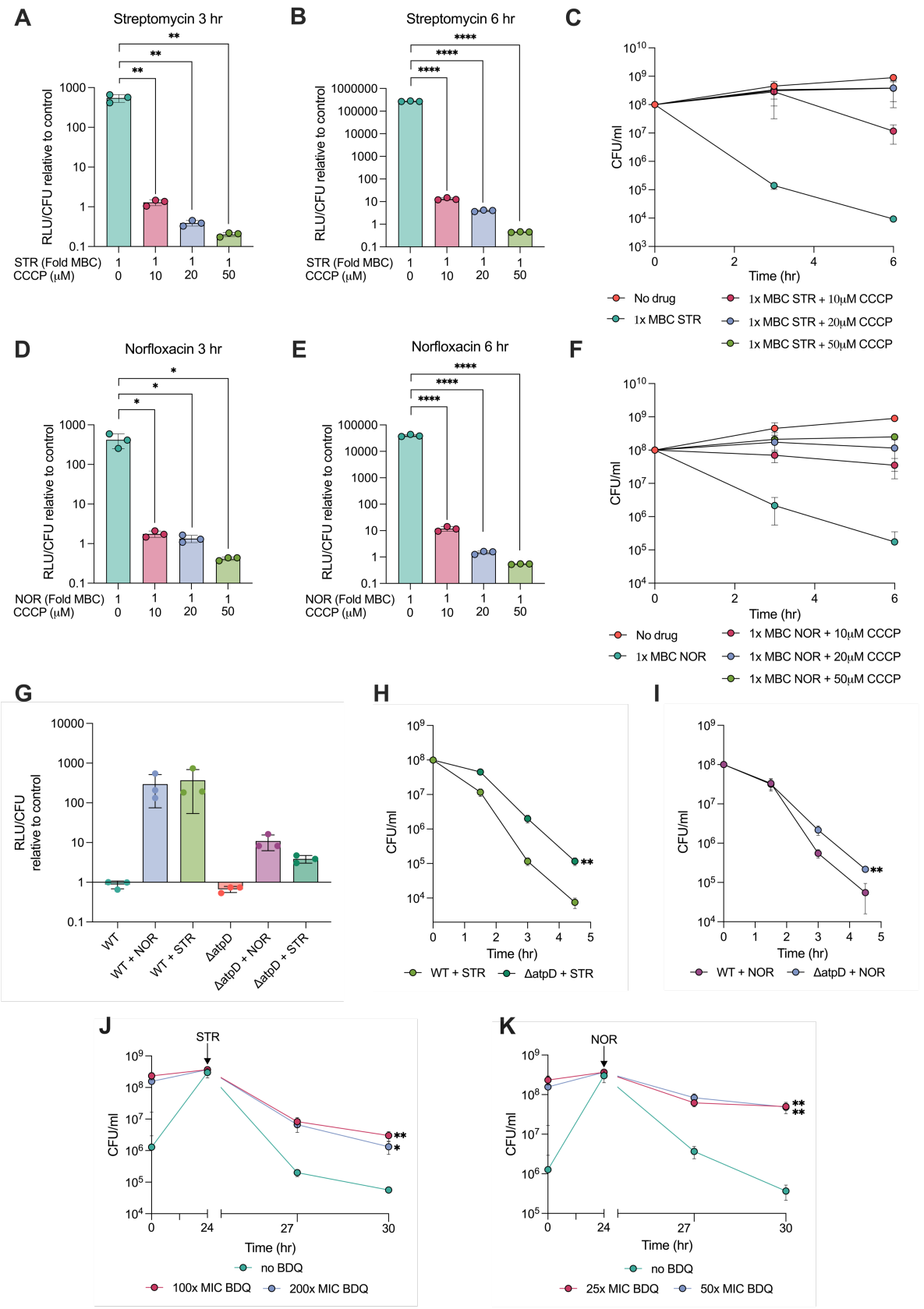

Fig. 6. Inhibition of excess ATP production mitigates antibiotic lethality. Bar graphs reports the dose-dependent reduction in ATP levels upon CCCP co-treatment with STR (A and B) and NOR (D and E). The effect of increasing concentrations of CCCP on survival of *M. smegmatis* challenged with lethal dose of STR (C) and

NOR (F), respectively. Bar graphs represent the relative luminescence measurements indicating ATP levels in wild-type and Δ*atpD* in response to 1x MBC_{99} of STR and NOR for 3 hours (G). Time kill curves demonstrate the survival differences of wild-type and Δ*atpD* in response to 1x MBC_{99} of STR (H) and NOR (I). Figures (J and K) depict time-kill curve of *M.smegmatis* pre-treated with BDQ for 24 hours, and subsequently challenged with STR and NOR, respectively. 1x MIC_{99} of BDQ used in the study was 0.0075 µg/ml. All data points represent the mean of at least three independent replicates ± SD. Statistical significance was calculated by students' t-test (unpaired), *$p < 0.05$, **$p < 0.01$, ***$p < 0.001$, ****$p < 0$.

ATP burst is the dominant driver of antibiotic lethality in mycobacteria.

After demonstrating that inhibiting either ROS generation or excess ATP production can inhibit antibiotic-induced cell death, we sought to determine which of these two mechanisms is the dominant driver of lethality. ROS levels were compared under the conditions of ATP burst formation (antibiotic treatment alone) and ATP burst mitigation (antibiotic plus CCCP co-treatment). We reasoned that if damage by ROS is the dominant mechanism driving cell death, then co-treatment with CCCP would decrease ROS levels to impart enhanced survival in the presence of antibiotics. In our observation, antibiotic treatment alone increased oxidative stress due to ROS and caused cell death in the case of both antibiotics **(Fig. 7A to 7D)**. Intriguingly, while CCCP-mediated inhibition of ATP burst increased cell survival, 405/488 nm ratio (oxidative stress) remained higher in the surviving cells, indicating that the ATP burst, and not ROS production, is the dominant mechanism driving antibiotic lethality in mycobacteria. Our results also suggest that oxidative stress alone, a correlate of ROS levels, is insufficient to cause cell death. It points out that ROS is a by-product of antibiotic action (i.e., enhanced respiration) rather than the predominant secondary mediator of cell death, as originally understood. Notably, the CCCP-mediated increase in respiration was also evident from a dose-dependent increase in 405/488 nm ratios with CCCP treatment alone **(S5G and S5H)**. In summary, our results show that NOR and STR treatments increase respiration, resulting in a lethal ATP burst that mediates mycobacterial death.

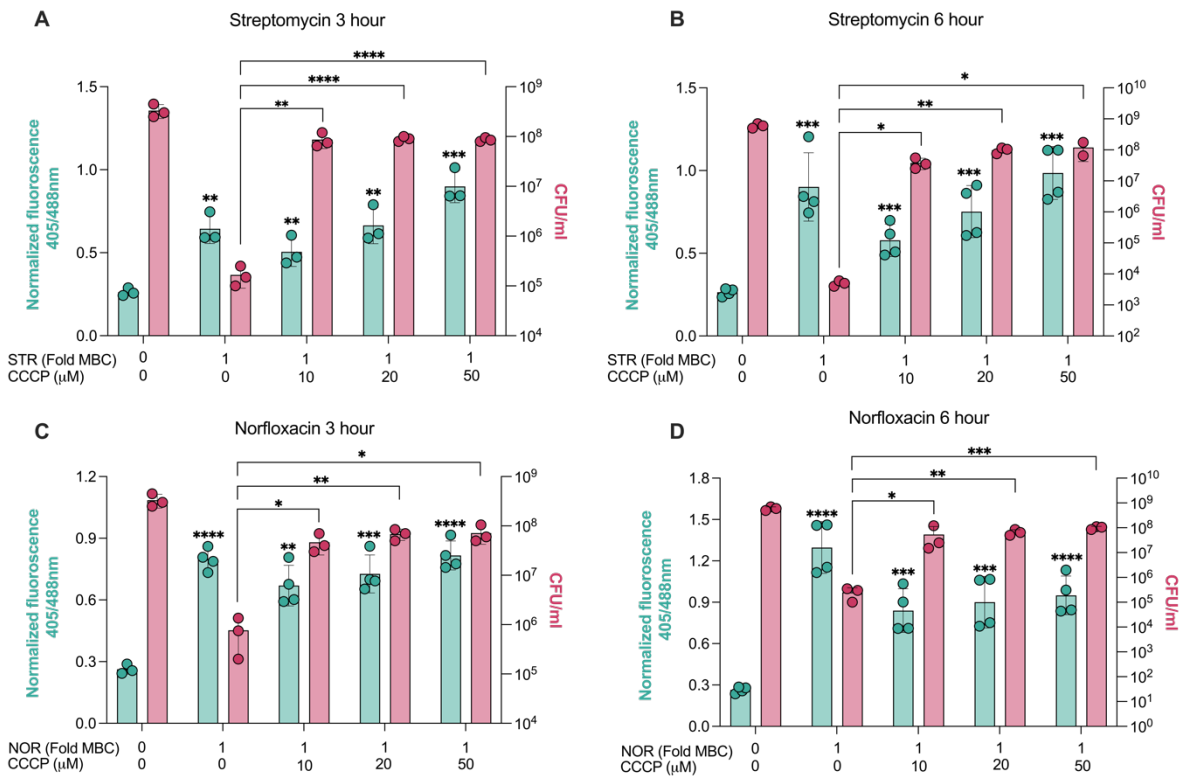

Fig. 7. Norfloxacin and streptomycin induced ROS is insufficient to mediate cell death. Ratiometric response of *M. smegmatis* expressing Mrx1-roGFP2 redox biosensor (left y-axis) and the cell viability (right y-axis) in response to STR (A & B) and NOR (C & D) with and without the co-supplementation with CCCP post 3 hours and 6 hours of treatments. Data points represent the mean of at least three independent replicates ± SD. *p < 0.05, **p < 0.01, ***p < 0.001, ****p < 0.0001 by students' t-test (unpaired).

Antibiotic-induced ATP burst deprives cells of essential divalent metal ions.

ATP synthesis is essential for optimal growth and survival against stresses in all living organisms. Therefore, the involvement of ATP in cell death is difficult to comprehend. However, ATP is known to bind and chelate various divalent metal ions (20–22) and intriguingly, a study reported growth inhibitory activity of exogenously supplied ATP on multiple bacterial species, which were rescued upon co-treatment with magnesium and iron salts(23). Based on these studies, we hypothesized that the ATP burst observed upon antibiotic treatment may have sequestered and deprived the macromolecules and cellular processes of their essential divalent metal ions, resulting in cell death. Towards this end, we first established whether metal ion chelation alone is lethal to cell survival. Since the metal ion chelators, EDTA and EGTA are not taken up by Mycobacteria, as a proof-of-concept, we employed the cell permeable iron chelator, bipyridyl (BP), to test whether intracellular iron depletion causes

bacteriostasis or cidality. The *M. smegmatis* strain challenged with increasing concentrations of bipyridyl displayed a dose-dependent killing **(Fig. 8A)**, demonstrating that iron removal causes cell death. Next, we reasoned that if ATP burst-mediated cell death was due to metal ions depletion, then exogenous supplementation of divalent metal ions should increase bacterial survival to antibiotics. To test this, we compared cell survival upon NOR or STR treatment with and without the co-supplementation of four different divalent metal ions: Fe^{2+}, Mg^{2+}, Mn^{2+}, and Zn^{2+}. We observed a concentration-dependent protection from antibiotics provided by all four metal ions, suggesting that ATP burst-mediated divalent metal ion chelation confers antibiotic lethality **(Fig. 8B to 8E)**. A similar level of protection was not achieved from monovalent metal ions **(S6)**. A decrease in cell survival observed with 10 mM Fe^{2+} could be attributed to Fenton cycle mediated ROS generations that may have occurred due to excessive free iron in the cells. Separately, we also tested whether divalent metal ion supplementation is toxic to cells and causes growth arrest, leading to increased cell survival. Notably, a salt concentration of 5 mM that provided near complete protection against antibiotics had no adverse effect on the bacterial growth rate **(Fig. 8F)**, and thus, the enhanced survival obtained with salt co-treatment was not due to growth arrest.

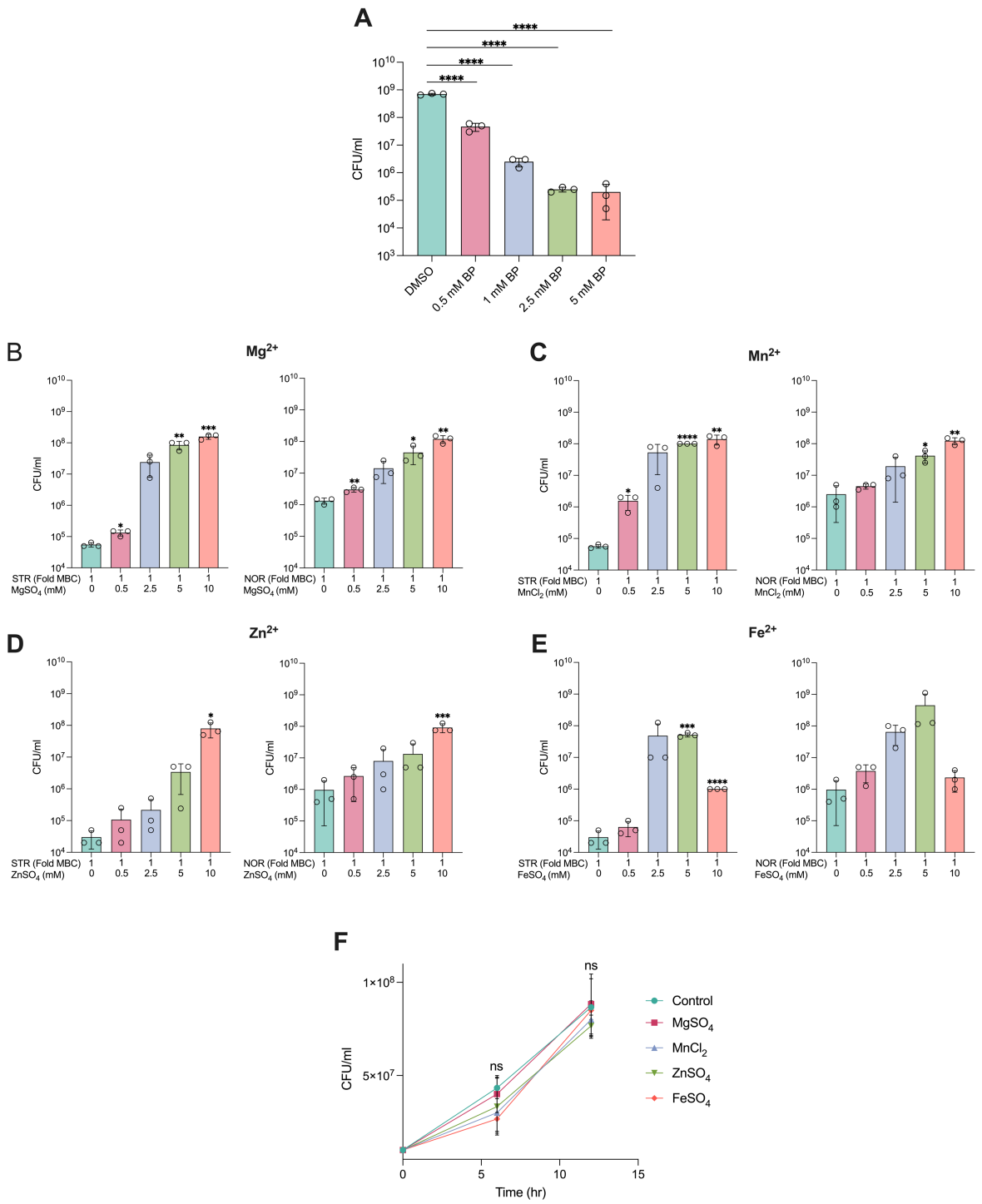

Fig. 8. Antibiotic induced ATP levels chelates divalent metal ions. (A) Effect of increasing concentrations of bipyridyl (BP) on the survival of *M. smegmatis* (0.8 OD/ml). Bar graphs indicate the effect of increasing concentrations of $MgSO_4$ (B), $MnCl_2$ (C), $ZnSO_4$ (D), and $FeSO_4$ (E) on the survival of *M. smegmatis* challenged with lethal dose of the antibiotics. Growth curve (F) showing the effect of 5 mM of $FeSO_4$, $MgSO_4$, $MnCl_2$, $ZnSO_4$ on the survival of *M. smegmatis.* Data points represent the mean of at least three independent replicates ± SD. Statistical significance was calculated using students' t-test (unpaired). *$p < 0.05$, **$p < 0.01$, ***$p < 0.001$, ****$p < 0.0001$.

^{13}C isotopomer analysis suggests increased metabolic flexibility and bifurcation of TCA cycle flux as a bacterial adaptive mechanism.

After studying the nature of antibiotic-induced stresses, we sought to investigate bacterial counter responses that could promote adaptation to antibiotics and growth recovery. ^{13}C isotopologue profiling was performed to investigate the metabolic rewiring that promotes the resumption of growth during the recovery phase. Using ^{13}C glucose as a carbon tracer, intracellular metabolites from central carbon metabolism (at t = 25 hr, treated with ¼x MBC_{99} of NOR or STR) were assessed. In agreement with the proteomics data, there was an increase in citrate flux **(Fig. 9A)** that correlated with the upregulation of citrate synthase **(Fig. 3F)**. Similarly, there was an increase in flux through the oxidative segment of the TCA cycle and towards alpha-ketoglutarate/glutamate production, which correlated with the observed increases in aconitase and isocitrate dehydrogenase levels. The time-dependent increase in the ratio of NADH/NAD+ under NOR and STR treatments **(Fig. 9B)** and a dose-dependent increase with STR treatment **(Fig. 9C)** further confirmed the increased flux measurements through the TCA cycle. The observed increase in the levels of NADH, as also confirmed by mycobacteria specific *in vivo* NADH biosensor, Peredox (**S7A**) (24), can fuel the ETC chain further to enhance the production of ATP and generate ROS as a by-product. Collectively, our measurements of increased respiration, ROS generation, and ATP production could be explained by an increase in flux through the TCA cycle, following sub-lethal antibiotic treatment.

The decreased flux into pyruvate indicates that phosphoenolpyruvate carboxykinase (PckA), that was upregulated in the proteomic analysis **(Fig. 3F)**, is operating in the anaplerotic direction to fix CO_2 to form oxaloacetate (OAA). It has been demonstrated that the redox state of the cells influences the reversal of PEPCK activity and has been associated with increased ROS production (25). This finding was further corroborated by the increase in the aspartate label (a surrogate for oxaloacetate) and the M+3 and M+5 ionic species of ^{13}C-citrate **(S7B and S7C)**. This increased flux into OAA can facilitate greater utilization of acetyl-CoA by the TCA cycle, as indicated by the increased label of citrate. Since antibiotic-mediated death was caused by increased respiration, ROS, and ATP levels we expected that bacteria exposed to sub-lethal doses of antibiotics may remodel their central carbon metabolism (CCM) to minimize respiration and improve their chances of survival. In agreement with this hypothesis, the enhanced flux in the oxidative arm of the TCA cycle (alpha-ketoglutarate) was found to diverge towards glutamate, glutamine, and GABA shunt following streptomycin treatment **(Fig. 9A)**.

This deviation of the flux was facilitated by upregulation of glutamate dehydrogenase, glutamate synthase, glutamine synthetase, and glutamate decarboxylase, as evident from the proteomics data **(Fig. 3F)**. The amino acids glutamate and glutamine direct the carbon flux to amino acid biosynthesis and help regulate energy and nitrogen metabolism (26–28). In addition, increased flux in glutamate and GABA would help bypass two enzymatic reactions of the TCA cycle's oxidative arm, restricting ROS production and regulating anaplerosis (29,30). Moreover, we observed an increased flexibility of the TCA cycle in switching carbon flux from aspartate/oxaloacetate to alpha-ketoglutarate/glutamate in response to antibiotics. This reaction is catalysed by aspartate aminotransferase (AspAT) which keeps balance between the cataplerosis and anaplerosis of TCA cycle intermediates in mycobacteria(31). AspAT was also found upregulated in our proteomics analysis. Overall, our results suggest that by enhancing expression and activity of TCA cycle enzymes and those of the anaplerotic node (32), the antibiotic-adapted central carbon metabolism shows more plasticity and resilience in terms of minimizing the production of ROS and ATP, while still maintaining the overall metabolism and growth.

The glyoxylate shunt and PPP pathway were found to be involved in antibiotic tolerance mechanisms(33–35). We observed a decrease in the incorporation of ^{13}C label into succinate, indicating a decreased flux through succinate-semialdehyde dehydrogenase (SSADH), alpha-ketoglutarate dehydrogenase (KGDH) or isocitrate lyase (ICL1). Antibiotic treatments decreased the expression of the sucA and sucB subunits of KGDH and the gabD1 and gabD2 subunits of SSADH, explaining the lower flux in succinate. Furthermore, there were no changes in the ^{13}C label in histidine and sedoheptulose 7-P indicating that flux through the PPP remained unperturbed upon antibiotic treatment **(S7D)**. Since the enzymes of the oxidative stage (G6-PDH and 6-PGD) were found upregulated in our proteomics analysis it may be speculated that the flux from ribose 5-phosphate got channelized towards purine biosynthesis. The NADPH/NADP+ ratio measurements also revealed no significant differences in antibiotic treated cells (**Fig. 9D and 9E)**. Overall, no changes in flux into the PPP and glyoxylate shunt were observed during the antibiotic exposure.

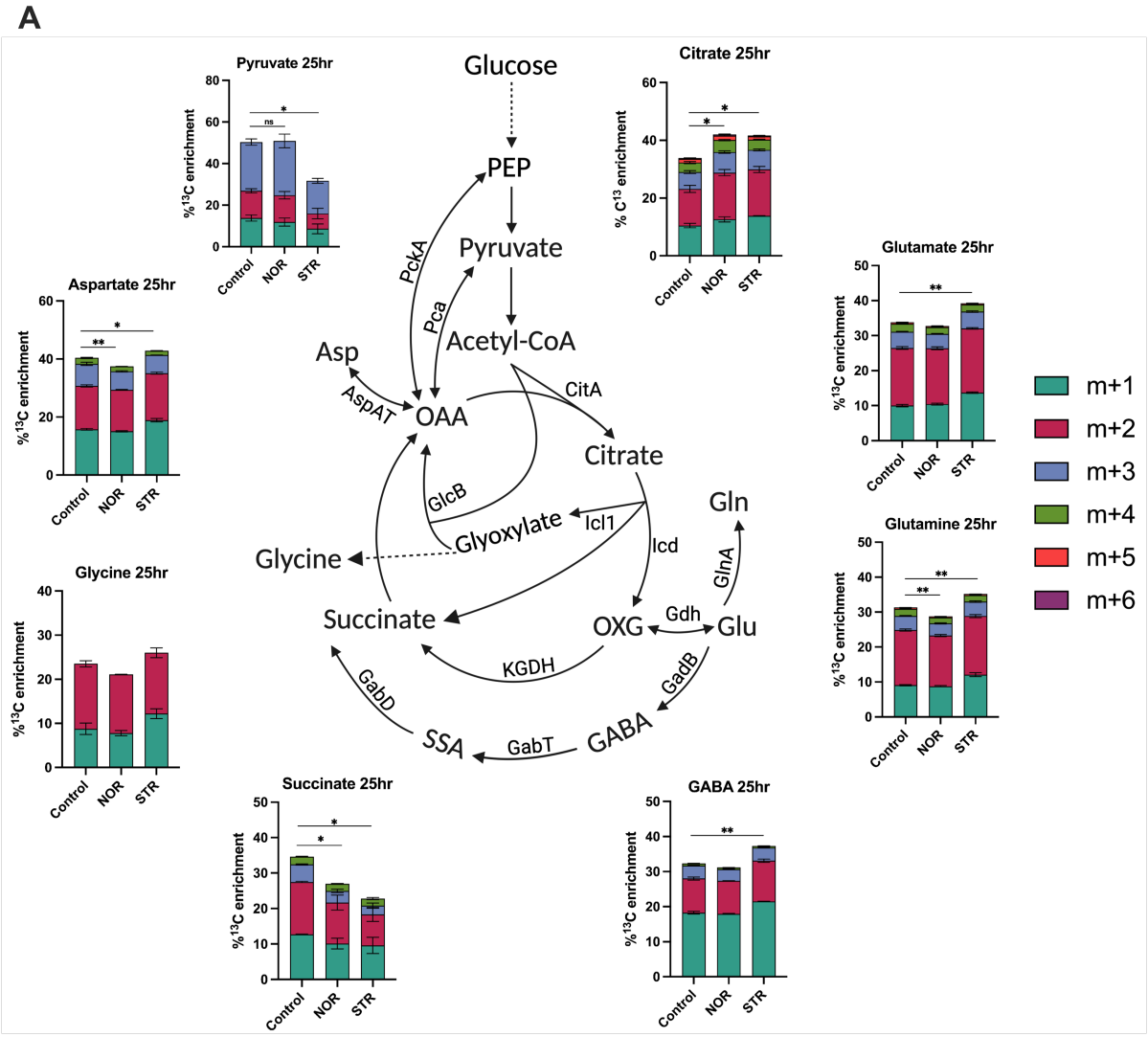
A
Glucose
PEP
Pyruvate
Acetyl-CoA
PckA
Pca
Asp
AspAT
OAA
CitA
Citrate
GlcB
Glyoxylate
Icl1
Icd
Gln
GlnA
Glycine
Succinate
OXG
Gdh
Glu
KGDH
GadB
GabD
SSA
GabT
GABA
Pyruvate 25hr
Citrate 25hr
Aspartate 25hr
Glutamate 25hr
Glycine 25hr
Glutamine 25hr
Succinate 25hr
GABA 25hr
% 13C enrichment
Control
NOR
STR
m+1
m+2
m+3
m+4
m+5
m+6

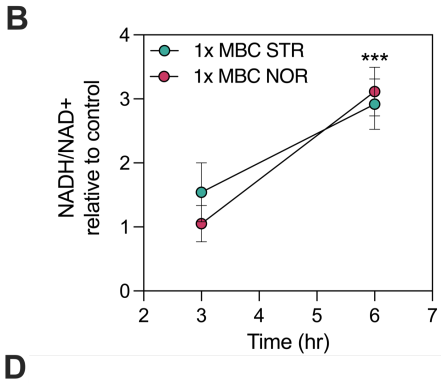
B
1x MBC STR
1x MBC NOR
***
NADH/NAD+ relative to control
Time (hr)

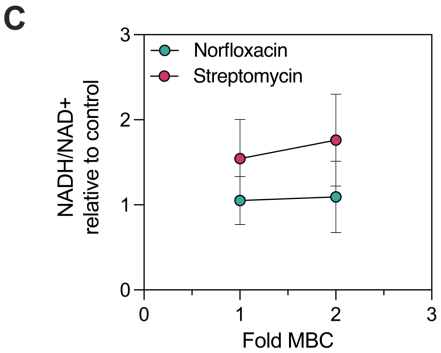
C
Norfloxacin
Streptomycin
NADH/NAD+ relative to control
Fold MBC

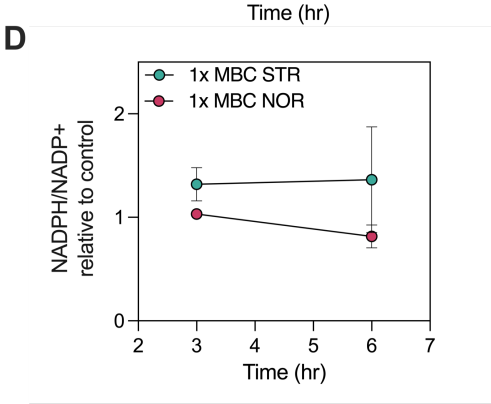
D
1x MBC STR
1x MBC NOR
NADPH/NADP+ relative to control
Time (hr)

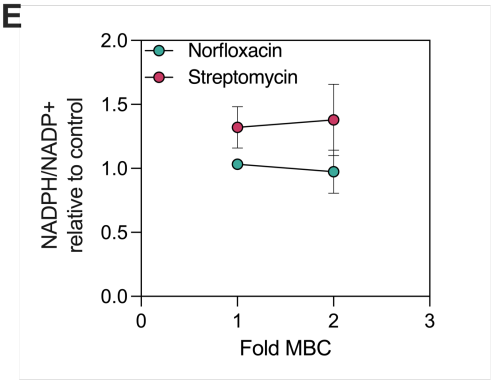
E
Norfloxacin
Streptomycin
NADPH/NADP+ relative to control
Fold MBC

Fig. 9. ^{13}C metabolomics suggests increased metabolic flexibility and bifurcation of TCA cycle flux as bacterial adaptive mechanism. (A) Percent ^{13}C enrichment in CCM metabolites of *M. smegmatis* challenged with ¼x MBC_{99} of antibiotics at 25 hour time point (recovery phase). "M" denotes the molecular mass of the metabolites, where M+1(n) denotes the incorporation of ^{13}C labelled carbon in the metabolites, leading to increase in the mass by that extent. Data for each isotopologue are represented as mean ± SD from independent triplicates. PEP, phosphoenolpyruvate carboxykinase; OXG, alpha-ketoglutarate; Glu, glutamate, Gln, glutamine, OAA, oxaloacetate; Asp, aspartate; GABA, γ-Aminobutyric acid, SSA, succinic semialdehyde. Line graphs represent the ratios of NADH/NAD+ and NADPH/NADP+ with time (B,D) and dose-dependent manner (C,E), respectively, after antibiotic treatments. Data points represent the mean of at least three independent replicates ± SD. *$p < 0.05$, **$p < 0.01$, ***$p < 0.001$ were calculated by student's t-test (unpaired).

Sub-lethal antibiotic exposure can potentiate development of tolerance and genetic resistance to antibiotics

Next, we questioned whether sublethal antibiotic concentrations have activated any intrinsic drug resistance mechanisms. Specifically, proteomics data analysis revealed a 50-fold upregulation of the protein Eis at 25 hours after STR treatment **(Fig. 10A)**. Eis is known to acetylate and inactivate aminoglycosides, thus conferring antibiotic tolerance and promoting enhanced intracellular survival (16,36). This provides evidence that mycobacteria may induce intrinsic mechanisms to adapt to sub-lethal antibiotic exposure.

To test whether sub-lethal antibiotic concentrations increase mutation frequency, we performed a classical Luria-Delbruck fluctuation test using rifampicin resistance as the phenotypic reporter. We harvested cells from the recovery phase (25th hour) and compared the number of rifampicin resistant mutants in NOR/STR-treated versus untreated conditions. Within 22.5 hours of antibiotic exposure, the mutation frequency of cells adapted to sub-lethal concentrations of STR increased by 4-fold, whereas NOR treatment did not significantly increase the mutational frequency **(Fig. 10B)**. These findings indicate that antibiotic-induced physiological adaptation may facilitate the acquisition of drug-specific qualitative mutations or non-specific quantitative mutations in metabolic enzymes, leading to antibiotic resistance and treatment failure.

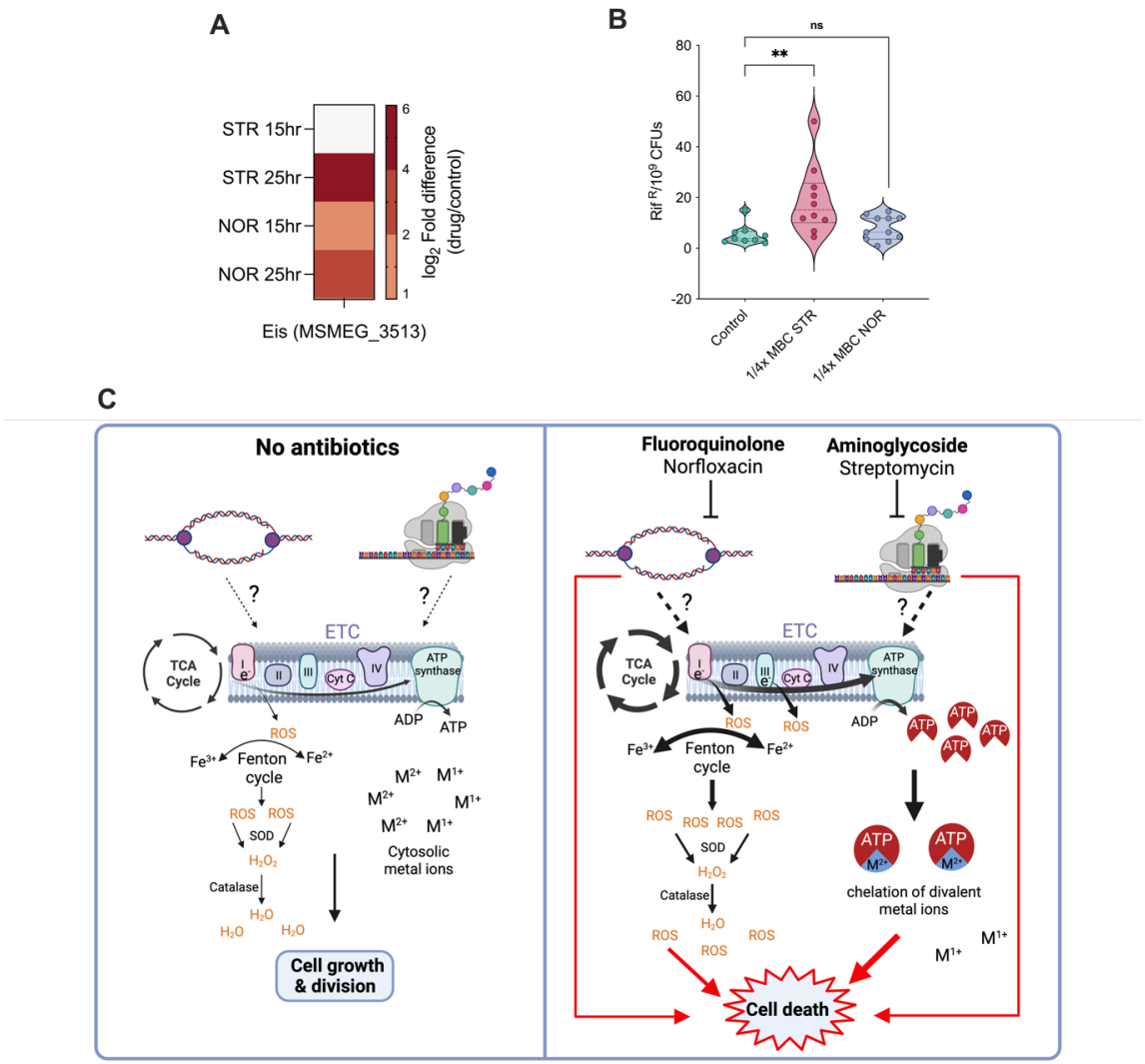

Fig. 10. Sub-lethal antibiotic exposure can potentiate development of antibiotic resistance. Heat map (A) showing the $\log_2$ fold differences of protein Eis in response to antibiotic treatment. Figure (B) depicts the mutational frequency of *M. smegmatis* grown in ¼ x MBC_{99} of the antibiotics for 25 hours; each dot represents the mutational frequency of one replicate (n = 10). *p < 0.05, **p < 0.01, ***p < 0.001 were calculated by student's t-test (unpaired). (C) Proposed model of antibiotic lethality in Mycobacterium. Figure on left explains the interaction among the central dogma processes and central carbon metabolism (CCM), where, depending on the need for energy, flux through CCM is modulated leading to optimal growth and division; Figure on right explains the effect of inhibition of essential cellular processes by antibiotics, resulting in activation of CCM and respiration, leading to ROS generation and ATP burst. Elevated ATP levels chelate essential divalent metal ions and deny them as co-factors for various proteins, eventually leading to cell death. The thickness of arrows indicate the impact of the processes.

Discussion:

The current understanding of antibiotic lethality is limited to target corruption as the primary cause and free radical induced cellular damage as a secondary consequence. This study while

explores the mycobacterial responses to antibiotics, identifies ATP burst as the new and dominant driver of antibiotic-induced cell death in mycobacteria. Our differential proteomics analysis upon antibiotic exposure, revealed a rewiring in the central carbon metabolism and generation of an anti-oxidant response due to the production of ROS. Damage by ROS has been proposed as an universal mechanism that many bactericidal antibiotics use to eliminate bacteria, irrespective of their primary targets(2). Respiration inducing molecules such as Vitamin C, N-acetylcysteine (NAC), and other thiols were found to use ROS to enhance antibiotic lethality, even against drug induced-persisters while ROS quenching by antioxidants rescued bacteria from cell death (11,14,34,37,38). Our measurements revealed upregulated central carbon metabolism enzymes, increased flux through the TCA cycle, high NADH/NAD+ ratios, and elevated ROS levels in response to even sub-inhibitory concentrations of antibiotic. Notably, the set of bacterial responses were shared by norfloxacin and streptomycin which belong to two distinct class of drugs, the fluroquinolones and aminoglycosides, respectively. Thus our observations further strengthen the evidence of increasing involvement of ROS in antibiotic action and also in inducing tolerance in bacterial pathogens, including mycobacteria(11,34,39,40)

While electron leakage from the ETC is the primary source of ROS, it is unclear how antibiotics are sensed beyond their primary targets and how they modulate the ETC to generate additional ROS. Recent studies have demonstrated that antibiotics deplete the purine nucleotide pool, resulting in an increase in purine biosynthesis and hence ATP demand (41,42). This increased energy demand becomes a signifcant reason for increased respiration, oxygen consumption, and ROS generation, thus contributing to enhanced antibiotic lethality(41). To confirm that increased respiration led to ROS production, we directly measured ATP levels, the end product of aerobic respiration. Both norfloxacin and streptomycin treatments resulted in a substantial dose- and time-dependent rise in ATP levels that was inversely proportional to cell survival. By inhibiting antibiotic-induced ATP burst using a protonophore uncoupler of ETC and oxidative phosphorylation (CCCP), an inhibitor of ATP synthesis (Bedaquiline), or the ATP deficient Δ*atpD* strain (genetic uncoupler), we showed that the observed increase in ATP concentration was due to enhanced oxidative phosphorylation, and significantly contributed to antibiotic action and cell death.

Growth rate and metabolism were shown to influence antibiotic efficacy (43–45). A previous study concluded that the bacterial metabolic state, not the growth rate, is the primary driver of cidality (46). In addition to increased respiration, our proteomics analysis revealed

that downregulation of ATP-consuming processes, such as the central dogma and cell division, could be contributing to this ATP accumulation. Thus energy metabolism and particularly ATP synthesis, becomes a central component of the connection between metabolic state and antibiotic susceptibility. Recent studies have observed a remarkable correlation between lower ATP levels and generation of persister population in *S. aureus* and *E.coli* (47,48). Interestingly, exogenous supplementation of alanine or glucose increased the susceptibility of drug-resistant *E. tarda* by boosting the flux through the TCA cycle and increasing the proton motive force, resulting in increased kanamycin uptake(49). Based on these observations, it may be logical to reason that inhibition of oxidative phosphorylation would result in reduced antibiotic cidality and reveal a plausible direct role of ATP in determining antibiotic susceptibility. Supporting this hypothesis, cell wall acting antimycobacterials were shown to increase ATP levels in *M. bovis BCG*, which directly correlated with antibiotic efficacy (50). Furthermore, energy metabolism inhibitors, bedaquiline and telacebec were found to dampen the bactericidal activity of isoniazid and moxifloxacin against *M. bovis BCG* and *M. tuberculosis* (51).

Since inhibition of either ROS generation or ATP burst was sufficient to reduce the lethality of norfloxacin and streptomycin, we sought to determine which of the two is the dominant contributor. Intriguingly, measurements of ROS in CCCP-protected mycobacteria revealed that elevated ROS levels were insufficient to cause cell death upon antibiotic treatment, in the absence of an ATP burst, indicating that ATP burst is the dominant mechanism driving cell death. Conditions such as hypoxia, stationary phase, nutrient starvation, biofilm formation (33,52,53) or an artificial reduction of the NADH/NAD+ ratio (11) renders mycobacteria less susceptible to antibiotics compared to actively growing cells, and this phenotype has been attributed to lower levels of ROS. Based on our findings, we are tempted to hypothesize that these conditions would also generate lesser flux through the electron transport chain (respiration), which, in addition to decreasing ROS levels, would also produce lower levels of ATP. Since the metabolic rate, ROS, and ATP burst are interrelated, studying their individual contributions remains challenging but necessary. We show that in the absence of an ATP burst, mycobacteria can tolerate the consequences of primary target inhibition and the damage from ROS for a longer duration, which is insufficient for cell death. Contrary to our observations, a genetic uncoupling of ATP synthesis potentiated lethality in *E. coli*, indicating that enhanced respiration and ROS production is the dominant driver of efficacy for bactericidal antibiotics (54). These findings suggest similarities in the bacterial metabolic tool kit exploited by cidal antibiotics while targeting across genera, yet identify the differences in

the pivotal component that drives cell death in *M. smegmatis*. Therefore the secondary mechanisms of lethality should be tested for a panel of bactericidal antibiotics, with distinct mode of action, across different bacterial pathogens including *M. tuberculosis*, which is an intriguing lacunae of our study. Likewise, while we note the commonality in the involvement of ROS and ATP burst in fluoroquinolones and aminoglycoside action, we highlight that the extent of ROS and ATP's contribution may differ between the two antibiotics. The levels of ROS produced were higher for norfloxacin, whereas the extent of ATP burst was greater for streptomycin, which demanded additional bedaquiline to suppress the streptomycin induced ATP burst and killing.

Metal ion binding by ATP is a well-known phenomenon, where ATP forms a stable coordination complex with the metal ion(21,22,55). We discovered that co-supplementation with divalent metal ions rescued mycobacteria from the cidality of STR and NOR. Further, exogenous supplementation with ATP was found to cause bacteriostasis in various bacteria, including mycobacteria (23). Based on this observation, we propose metal ion chelation and depletion by ATP burst as a novel bactericidal mechanism executed by antibiotics in mycobacteria. We have separately established that the depletion of Fe^{2+} is lethal in mycobacteria, suggesting the essentiality of these cofactors for survival. Future studies should investigate the antimicrobial role of ATP dependent chelation of metal ions beyond iron, evaluating the effect of intracellular sequestration of other divalent metal ions using specific chelators. In conclusion, our study fills a gap and expands the current understanding of how antibiotics ultimately cause cell death in the context of mycobacteria. Whether other bactericidal antibiotics employ ATP burst to mediate their lethality in mycobacteria and other serious pathogens warrants further investigation. In conjunction, compounds that synthetically generate ATP burst should also be tested for antimycobacterial efficacy.

M.tuberculosis is an outlier among multi-drug resistant pathogens due to its low recombination rate, limited genetic diversity and absence of an accessory genome. Becoming a successful pathogen, despite its inability to rapidly evolve and withstand new antibiotics alludes to the presence of an effective innate mechanism of resistance. Low fitness-cost mutational events causing transient antibiotic tolerance in the absence of a strong selective pressure, precede and possibly boost successive qualitative mutations on antibiotic targets(4,5). In our observations, Mycobacterial counter responses included downregulation of central dogma and cell division processes thereby reducing the vulnerability of the target and thus efficacy of the antibiotic. Reduction of the energy consuming processes reduces the anabolic

demand and helps diminish their energy metabolism, ROS production and ATP systhesis ^{13}C isotopomer analysis revealed rerouting of flux from alpha-ketoglutarate to glutamate-glutamine and GABA, bypassing the oxidative arm of the TCA cycle. We also measured an increased mutation frequency and the induction of Eis, demonstrating that the antibiotic-adapted population may facilitate the selection of drug-resistant mutants (4,5,16,36). In summary, we observed that upon exposure to sub-inhibitory levels of antibiotics Mycobacterium transiently switched to a quiescent state that reduces its respiration thus denying the antimicrobial effect from metal ion chelation by ATP. These findings could be used to develop antibiotic adjuvants that enhance aerobic metabolism (56), and increase ROS mediated damage and ATP production. Our study also advocates for a thorough understanding of the proximate and ultimate causes of antibiotic lethality (57), in order to avoid drug combination with overlapping (secondary) actions and mechanism of tolerance.

Materials and Methods

Bacterial strains, growth conditions

Mycobacterium smegmatis MC^2155 (Msm) strain was grown in Middlebrook 7H9 broth (Difco) supplemented with 2% Glucose, 0.05% Tween-80 at 37-degree incubator at 200 rpm shaking or on Middlebrook 7H10 agar supplemented with 2% glucose. Msm cells were electroporated with Mrx1-roGFP2 or Peredox-mCherry biosensor and grown with 50 µg/ml of hygromycin. Msm cells were electroporated with PHR-mCherry (ATP/ADP sensor) plasmids, and grown with 20 µg/ml of kanamycin. All three biosensors constitutively express their respective sensor proteins under *hsp60* promoter and offer ratiometric measurements.

Determination of MIC_{99} and MBC_{99}

A secondary culture of Msm was grown till the exponential phase (0.6 OD/ml). MIC_{99} was determined by incubating Msm cells (OD = 0.0005/ml) with 2-fold serially diluted antibiotic concentrations for 36 hours. Percentage survival was measured by Alamar Blue assay. The drug concentration that inhibited 99% of bacterial growth was termed as MIC_{99}. For the determination of MBC_{99}, Msm cells from the exponential phase were challenged with various drug concentrations and incubated at 37 degrees in a 96 well plate for 24 hours. The drug concentration that killed 99% ($2\log_{10}$ fold killing) of the initial bacterial population was termed MBC_{99}. For the experiments requiring different initial inoculum, a corresponding MBC_{99} was determined to account for inoculum effect (that can influence the extent or duration of killing).

Growth curve of *M. smegmatis* with sub-lethal concentrations of norfloxacin and streptomycin

For the growth curve experiment, a tertiary culture of Msm cells was exposed to either 1x-MBC_{99} or ½x-MBC_{99} or ¼x-MBC_{99} concentrations of norfloxacin and streptomycin, individually, with starting inoculum of 0.0025/ml. Cultures were grown at continuous shaking conditions at 37 degrees. Drugs were added at 2.5 hours after the start of the growth curve. For the measurement of viability, cells were serially diluted and plated on LB agar at every 2.5 hour for a total of 25 hours. The experiment was repeated at least 6 times for both the antibiotics.

MIC verification

MIC verification was performed and compared between cells grown with and without the ¼x MBC_{99} concentrations of norfloxacin and streptomycin, individually, for a total of 25 hours. Cells were harvested from the 25 hours time point, and seeded into 96 well plates, pre-seeded with 2 fold serially diluted antibiotic concentrations. Percentage survival was plotted using Alamar Blue assay.

Quantitative Proteomics

Reagents: All reagents were purchased from Sigma Merk. Sequencing grade modified trypsin was purchased from Promega. All the MS grade solvents, water, acetonitrile, and formic acid were procured from Fisher chemicals.

Sample preparation: Proteomic analysis was performed as reported previously (58). For proteomics, cells were grown in 5 independent experiments each for drug treated and untreated conditions. Msm cells were harvested from desired time points and conditions at 6000 g at 4 degrees, washed thrice with chilled PBS (pH=7.4). The cell pellets were stored at -80 degrees until further use. Cell pellets were resuspended in 1ml of lysis buffer (PBS + protease cocktail inhibitor + 1mM EDTA) to minimise non-specific protein degradation. Cells were lysed by mechanical shearing in a bead-beater with at least 10 cycles (7m/s for 45 seconds) of lysis. Tubes were kept on ice for 3-4 minutes in-between the cycles. The supernatant of the cell lysate was precipitated using 1:4 v/v of TCA. Protein precipitates were solubilized in 6M urea and subsequently quantified using BCA kit (Sigma). Ten micrograms of the protein samples were reduced with 10mM dithiothreitol (DTT) and alkylated with 37 mM iodoacetamide (IAA). These linearised proteins in 50mM ammonium bicarbonate (pH = 7.8), were digested with a modified MS grade trypsin (Promega; 1:5 enzyme/protein) overnight at 37 °C. The reactions were terminated by the addition of 2 µl of trifluoroacetic acid (TFA) to bring pH < 2.

Peptide de-salting: Tryptic Peptides were desalted using custom-made stage tips employing the Empore™ C-18 disks. Stage-tips were conditioned and equilibrated with 100% acetonitrile and 0.1% formic acid in water, respectively, before sample loading. Peptides were washed with 0.1% formic acid, eluted using 50% acetonitrile in 0.1% formic acid. For LC-MS analysis, the samples were dried in a vacuum centrifuge to remove acetonitrile and resuspended in 0.1% formic acid.

LC-MS analysis: Peptides were analysed through Ultimate 3000 RSLC nano-UPLC system connected with an Orbitrap Elite hybrid mass spectrometer (Thermo Fisher Scientific). Roughly 600 ng of peptides were loaded with automated injections onto a trap column (Acclaim PepMap^{TM} 100, 3 µm particle size, 75 µm × 2 cm) for 4 min, at a flow rate of 5 µl min^{-1} with 0.1 % formic acid. The peptide separation was achieved on C-18 analytical column (PepMap^{TM} RSLC, 2 µm particle size, 100 Å pore size, 75 µm × 50 cm) at 250 nL min^{-1} flow rate, using the following solvents: solvent A, 0.1% formic acid in water; solvent B, 0.1% formic acid in 100% ACN. Both columns were equilibrated for 10 min with 5% solvent B. A slow gradient from 5% to 22% of solvent B was achieved in 85 minutes, which was then raised to 28% of solvent B in additional 20 mins. This was followed by a quick increase to achieve 80% of solvent B in 5 minutes and maintained there for additional 10 minutes before bringing back to 2% solvent B. The analytical column temperature was maintained at 40°C. A stable spray at a voltage of 1.8 kV was generated using the nano spray electron ionization source (Thermo Fisher Scientific). The capillary temperature was maintained at 275° C for effective nebulization. The masses were measured in the positive mode using the data-dependent acquisition (DDA). MS1 and MS2 spectra were acquired in Orbitrap (60,000 resolution) and in ion trap analyser (rapid scan mode), respectively. For tandem mass spectrometry, twenty most abundant parent ions were sequentially selected from the MS1 spectrum (350-2000 m/z) and fragmented by collision-induced dissociation (CID). For MS1, the maximum ion accumulation time was set at 100 ms with a limitation of $1x10^6$ ions, whereas for MS2 spectra, the ion accumulation time was limited to 50 ms with a target ion limitation set at $5x10^3$ ions. Peptide fragmentation was performed at 35% of normalized collision energy. Dynamic exclusion of 30 seconds was applied with a repeat count of 1 to avoid repeated analysis of the same peptide.

Protein Identification: 10 raw files for each set of samples (five drug-free control and five ¼x-MBC_{99} drug treated samples) were analysed together by Maxquant (version 2.0.3.0) using the reference proteome of *Mycobacterium smegmatis mc²155* (https://mycobrowser.epfl.ch/; version v3) through its internal peptide search engine Andromeda(59,60). The following parameters were used for the protein identification: maximum missed cleavages, 2; mass tolerance for first and main search, 20 and 4.5 ppm respectively; mass tolerance for fragment ion, 0.5 Da; variable modifications used were N-terminal acetylation and methionine oxidation; minimum unique peptide required for identification, 1; minimum peptide length 7; max. peptide mass, 4600 Da; PSM and protein identification FDR were fixed at 0.01; dependent peptide and match between run were enabled with a match time window of 0.7 min and alignment window of 20 min.

Relative protein quantification: The maxLFQ algorithm was enabled in Maxquant for the lable-free quantification (LFQ) of all proteins(61). The protein group files generated from Maxquant were subsequently analysed by Persues (Version: 1.6.2.2) (62). Proteins identified as contaminants, from reverse sequence database as well as through modified peptides were removed. LFQ intensities were log transformed (log_2) and grouped in two groups (drug free and drug treated). Pearson correlation was performed on LFQ intensities to check for the reproducibility and correlation among samples. From 5 independent replicates, 3 highly correlating replicates were chosen for differential expression analysis using volcano plot.

Proteins with the fold difference of ±2 with p value ≤ 0.05 were considered to be significantly dys-regulated proteins.

Exclusive expression analysis: Proteins having valid LFQ intensities in all 3 replicates of one condition and were completely absent in all the replicates of other condition, were termed as exclusively/specifically expressed in that particular condition. Similarly, proteins that were specifically repressed/absent in one condition over another, were identified. These proteins are of equal importance since they are only expressed or repressed in response to drugs.

Enrichment analysis

Proteins that were up-regulated as well specifically expressed in response to drugs were analysed by ClueGO, a Cytoscape plug-in, for the KEGG Pathway enrichment analysis(63). Only pathways that had p value less than 0.05 were processed further. Benjamini-Hochberg multiple correction test was applied and the pathways that were still significant ($p \leq 0.05$) were termed as significantly enriched pathways.

Measurement of oxidative stress (ROS)

Cells expressing Mrx1-roGFP2 biosensor were challenged with drugs and reagents at different concentrations, and fluorescence was measured at 405 nm and 488 nm excitation wavelengths for a single emission at 520 nm. The ratio of fluorescence intensities obtained at 405 nm and 488 nm (405/488 nm) for 20 mM CHP and 100 mM DTT were used to normalise the data(9). In response to drugs or other reagents, 405/488 nm ratio was monitored either temporally and for the end point in BioTek Synergy H1 Plate Reader using a black 96 well plate (Costar). Since the plate reader measurement requires a higher number of cells (100 µl of ~0.8 OD/ml), a separate MBC determination assay was performed to determine the MBC for 0.8 OD/ml culture density to account for inoculum effects.

Time-kill kinetics

For the Time kill kinetics, cells with 0.1 OD/ml (~2 x 10^7 CFU/ml) were challenged with different antibiotic concentrations (fold MBC) alone or with other co-supplements in 96 well plates at 37 degrees. At regular intervals, cells were aliquoted and diluted in 7H9 + 0.05% Tween-80, and plated on LB agar to enumerate CFUs. After 3-4 days, the colonies were counted manually and plotted as CFU/ml over the course of time to exhibit a time-kill curve.

Measurement of ATP, NADH/NAD+, and NADPH/NADP+ ratio

Cells (0.8 OD/ml) were challenged with various fold MBC concentrations (predetermined for OD 0.8/ml) of norfloxacin and streptomycin. The higher inoculum was taken to ensure sufficient viability of cells upon antibiotic treatment for the detection of ATP, NAD+ and NADP+.

Intracellular ATP levels were determined using the BacTiter-Glo Microbial Cell Viability Assay (Promega) as per manufacturer's instructions. For ATP measurement, cells from various conditions and time points were harvested and heat inactivated at 90 degrees for 30 minutes,

as performed elsewhere (64). 25 µl of each sample was mixed with the equal volume of a BacTiter-Glo reagent in a white flat-bottom 96 well plate (Corning). Samples were incubated in dark at room temperature for 5 minutes, and bioluminescence was measured in a microplate reader (BioTek Synergy H1). The emitted luminescence was divided with the number of viable cells determined just before the heat inactivation to express ATP levels per bacterium (RLU/CFU). The CFU normalised luminescence observed for drug free control was set as 1, and RLU/CFUs values obtained for various conditions were plotted relative to the control.

NADH/NAD+ and NADPH/NADP+ ratios were measured using the Bioluminescent NAD/NADH-Glo detection kit (Promega) and NADP/NADPH-Glo detection kit (Promega), respectively, as per manufacturer's instructions. Briefly, cells at desired conditions were lysed using 2 cycles of bead beating (7 m/s for 45 sec). The supernatant of lysate was cleared using the centrifugation and processed for the measurement of NAD+ or NADP+ and NADH or NADPH separately, and the ratio of luminescence for NADH/NAD+ and NADPH/NADP+ were plotted. The ratios obtained for controls were set as 1, and the ratios obtained for various conditions were plotted with respect to control.

Measurement of respiratory activity using resazurin

Measurement of metabolic/respiratory activity was performed as reported elsewhere(16). Briefly, cells were grown till exponential phase in 7H9, and treated with desired drugs and supplements. At indicated time points, 100 µl aliquots of cells were removed and seeded in a black wall 96 well plate (Costar). Resazurin was added to all wells at a final concentration of 30 µg/ml and incubated in dark at 37 degrees for 30 minutes. The quick conversion of resazurin to resorufin was measured in a plate reader at the excitation of 530 nm and the fluorescence emission of 590 nm. Fluorescence intensities were divided with CFUs, measured just before the addition of the resazurin to express respiratory activity per bacterium. CFU normalised fluorescence intensities acquired for control were set as 1 and CFU normalised intensities obtained for various conditions were plotted relative to the control. The ability of resazurin to differentiate cells with distinct metabolic activity was separately confirmed by comparing normalised fluorescence acquired for cells from exponential phase, PBS starved cells and heat killed cells.

Measurement of NADH using Peredox-mCherry biosensor

The Peredox/mCherry biosensor indicating NADH/NAD+ ratio(24) was electroporated in *M. smegmatis*. Cells were grown with hygromycin (50 µg/ml) to 0.8 OD/ml, and cells were challenged with varying concentrations of STR and NOR for 3 hours at shaking, and 50 µM CCCP was used as a control. 200 µl cell aliquots were transferred to a black wall 96 well plate (Costar). Fluorescence was recorded in a microplate reader (BioTek Synergy H1) for Peredox at 410 nm excitation and 510 nm emission, while mCherry fluorescence was recorded at 588 nm excitation and 610 nm emission. The ratio of fluorescence acquired at the excitation of 410 nm and 510 nm (410/588 nm) were calculated and plotted.

Measurement of ATP using PHR-mCherry biosensor

The PHR/mCherry biosensor indicating ATP/ADP ratio(15) was electroporated in *M. smegmatis*. Cells were grown with kanamycin (20 µg/ml) to 0.8 OD/ml, and cells were challenged with varying concentrations of STR and NOR for 3 hours at shaking, and 50 µM CCCP was used as a control. After 3 hours, 100 µl of cells were aliquoted and diluted with 1:10 volume of PBS-0.05% Tween-80, and analysed by flow cytometry (Beckman Coulter CytoFLEX LX). Mean fluorescence intensities (MFI) for PHR acquired at 488 nm excitation and 525 nm emission (B525-FITC-A) was divided by that of the mCherry acquired at 588 nm excitation and 610 nm emission (Y610-mCherry-A). The ratio of fluorescence acquired at the excitation of 410 nm and 510 nm (488/588 nm) were calculated and plotted.

Detection of ROS using CellROX Deep Red dye

M. smegmatis cells were challenged with increasing concentrations of norfloxacin and streptomycin and seeded in a black wall 96 well plate (Costar). After 3 hours of treatments, cells were treated with 5 µM of CellROX Deep Red dye and incubated in dark at 37 degrees for 40 minutes. Fluorescence was recorded at 645Ex/665Em (nm) in a microplate reader (BioTek Synergy H1).

Fluctuation test

Luria-Delbruck fluctuation test was performed to determine if the treatment with the sub-lethal (¼x-MBC_{99} concentrations of norfloxacin and streptomycin, individually) antibiotics increase mutation frequency of cells. 10 ml of exponentially growing cultures of Msm were treated with and without ¼x-MBC_{99} concentrations of norfloxacin and streptomycin for a total of 25 hours at shaking. At 25th hour, 50 µl of cells were serially diluted and plated on LB agar to count CFU/ml, and the rest of the cultures were harvested at 6000 g and resuspended in 300µl of 7h9 + 0.05% Tween-80. 300 µl of suspension was plated onto 2 LB agar supplemented with 100 µg/ml (5x-MIC of RIF on agar) of Rifampicin. Plates were incubated in dark for 4-5 days at 37 degrees, and colonies were counted. The colonies that appeared on LB-RIF plates were RIF resisters (Rif^r). Mutation frequency was calculated by dividing the number of RIF resisters with the total number of CFUs plated on the LB-RIF plate, and compared between control and drug treatment.

^{13}C isotopologue analysis

Metabolite extraction: The metabolites were extracted and analysed as described elsewhere(65). Briefly, Msm cells were grown till exponential phase (0.6 OD/ml) and diluted to the inoculum of 0.0025 OD/ml in 7h9 supplemented with 0.05% Tween-80, 1% w/v $^{12}C_6$-Glucose and 1% w/v U-$^{13}C_6$ Glucose (50% labelled glucose). Identical to the growth curve and proteomics experiments, antibiotics were added at 2.5 hours and cells were grown with and without ¼x-MBC_{99} concentrations of norfloxacin and streptomycin for a total of 25 hours with shaking. At 25th hour, cells were harvested and washed twice using chilled PBS at 4000 rpm

for 10 minutes. Cells were subsequently resuspended in a pre-chilled methanol:acetonitrile:water (2:2:1), and metabolites were extracted by mechanical lysis with 0.1 mm zirconia beads using FastPrep system (MP Bio) set at 2 cycles of bead beating at 6.5 m/s for 20 seconds. Lysate was spun at 14,000 rpm for 2 minutes in a refrigerated centrifuge. The supernatant was filtered using 0.2 µM cellulose acetate filters, and stored at -80 degrees until further use.

LC-MS analysis: The metabolites were separated using the Agilent InfinityLab Poroshell 120 HILIC-Z (2.1 × 100 mm, 2.7 µm (p/n 675775-924)) column, suitable for polar acidic metabolites. Chromatographic separation was performed using the mobile phase A (10 mM ammonium acetate in water at pH = 9) and mobile phase B (1.0 mM ammonium acetate at pH = 9) in 10:90 (v:v) water/acetonitrile. Both the solvents were supplemented with a 5 µM Agilent InfinityLab deactivator additive (p/n 5191-4506). The gradient used for the separation is as follows; flow rate of 0.5 ml/min: 0 min, 100% B; 0 to 11.5 min, 70% B; 11.5 to 15 min, 100% B; 12 to 15 min, 100% B; and 5-min of re-equilibration at 100% B. Accurate mass measurements were performed by the Agilent Accurate Mass 6545 Q TOF apparatus, connected in line with an Agilent 1290 Infinity II UHPLC. The mass measurement was performed in a negative-ion mode using the following parameters; capillary voltage, 3000 V; fragmentor voltage, 115 V, in centroid 4 GHz mode. The instrument offered mass measurement at less than 5 ppm error with a mass resolution ranging from 10,000 to 45,000 over the fixed m/z range of 121 to 955 atomic mass units. Metabolites were identified based on their accurate masses and their accompanying isotopes. The percent ^{13}C labelling of each metabolite was determined by dividing the summed peak height ion intensities of all ^{13}C-labeled species by the total ion intensity of both labeled and unlabeled ionic species using the Agilent Profinder version B.8.0.00 service pack 3.

Statistical analysis: All the experiments were performed independently at least thrice or more. All the data are represented as mean and the error bars represent the standard deviation. All statistical analyses were performed in Graphpad Prism 9. For the calculation of statistical significance, the student's t-test (unpaired, two tailed) was performed in a pair-wise manner (between control and the desired experiment), as indicated in the figures.

Acknowledgements:

We thank Profs. John Mckinney and Vikas Jain, IISER Bhopal for providing us with the gene deletion mutants of *M. smegmatis of icl1-2* and *atpD*, respectively. We thank Dr. Areejit Samal for insightful discussions. The authors thank Drs. Amit Singh and Ashwani Kumar for gifting us Mrx1-roGFP2 biosensor, and Peredox-mCherry and PHR-mCherry biosensors, respectively. The authors thank Annesha Adhikari and Rohit Satardekar for assistance in the experiments and Akanksha Agrawal for assistance with creating images. TL thanks CSIR, India for the doctoral research fellowship and the EMBO short-term scientific exchange fellowship. RM thanks DBT, Govt. of India for research funding (BT/PR20820/MED/30/1875/2017). DB thanks Biotechnology and Biological Sciences Research Council (BBSRC) (BB/T007648/1) for research funding.

Competing interests: The authors declare that they have no conflict of interest.

References:

1. Tagliabue A, Rappuoli R. Changing Priorities in Vaccinology: Antibiotic Resistance Moving to the Top. Front Immunol [Internet]. 2018 May 30 [cited 2023 Aug 24];9(MAY):1068. Available from: /pmc/articles/PMC5992407/

2. Kohanski MA, Dwyer DJ, Hayete B, Lawrence CA, Collins JJ. A common mechanism of cellular death induced by bactericidal antibiotics. Cell [Internet]. 2007 Sep 7 [cited 2023 Aug 24];130(5):797–810. Available from: https://pubmed.ncbi.nlm.nih.gov/17803904/

3. Lobritz MA, Belenky P, Porter CBM, Gutierrez A, Yang JH, Schwarz EG, et al. Antibiotic efficacy is linked to bacterial cellular respiration. Proc Natl Acad Sci U S A [Internet]. 2015 Jul 7 [cited 2023 Aug 24];112(27):8173–80. Available from: https://www.pnas.org/doi/abs/10.1073/pnas.1509743112

4. Kohanski MA, DePristo MA, Collins JJ. Sublethal Antibiotic Treatment Leads to Multidrug Resistance via Radical-Induced Mutagenesis. Mol Cell. 2010 Feb 12;37(3):311–20.

5. Levin-Reisman I, Ronin I, Gefen O, Braniss I, Shoresh N, Balaban NQ. Antibiotic tolerance facilitates the evolution of resistance. Science [Internet]. 2017 Feb 24 [cited 2023 Aug 24];355(6327):826–30. Available from: https://pubmed.ncbi.nlm.nih.gov/28183996/

6. Global Tuberculosis Report 2022 [Internet]. [cited 2023 Aug 24]. Available from: https://www.who.int/teams/global-tuberculosis-programme/tb-reports/global-tuberculosis-report-2022

7. Moreno-Gámez S, Kiviet DJ, Vulin C, Schlegel S, Schlegel K, Doorn GS Van, et al. Wide lag time distributions break a trade-off between reproduction and survival in bacteria. Proc Natl Acad Sci U S A [Internet]. 2020 Aug 4 [cited 2023 Aug 16];117(31):18729–36. Available from: https://www.pnas.org/doi/abs/10.1073/pnas.2003331117

8. Dwyer DJ, Belenky PA, Yang JH, Cody MacDonald I, Martell JD, Takahashi N, et al. Antibiotics induce redox-related physi. Proc Natl Acad Sci U S A [Internet]. 2014 May 20 [cited 2023 Aug 24];111(20):E2100–9. Available from: https://www.pnas.org/doi/abs/10.1073/pnas.1401876111

9. Bhaskar A, Chawla M, Mehta M, Parikh P, Chandra P, Bhave D, et al. Reengineering Redox Sensitive GFP to Measure Mycothiol Redox Potential of Mycobacterium tuberculosis during Infection. PLoS Pathog [Internet]. 2014 Jan [cited 2023 Aug 24];10(1):e1003902. Available from: https://journals.plos.org/plospathogens/article?id=10.1371/journal.ppat.1003902

10. Saito K, Mishra S, Warrier T, Cicchetti N, Mi J, Weber E, et al. Oxidative damage and delayed replication allow viable Mycobacterium tuberculosis to go undetected. Sci Transl Med [Internet]. 2021 Nov 24 [cited 2023 Aug 24];13(621):2612. Available from: https://www.science.org/doi/10.1126/scitranslmed.abg2612

11. Shee S, Singh S, Tripathi A, Thakur C, Kumar AT, Das M, et al. Moxifloxacin-Mediated Killing of Mycobacterium tuberculosis Involves Respiratory Downshift, Reductive Stress, and Accumulation of Reactive Oxygen Species. Antimicrob Agents Chemother [Internet]. 2022 Sep 1 [cited 2023 Aug 27];66(9). Available from: https://pubmed.ncbi.nlm.nih.gov/35975988/

12. McBee ME, Chionh YH, Sharaf ML, Ho P, Cai MWL, Dedon PC. Production of superoxide in bacteria is stress- and cell state-dependent: A gating-optimized flow cytometry method that minimizes ROS measurement artifacts with fluorescent dyes. Front Microbiol. 2017 Mar 21;8(MAR):257948.

13. Balaban NQ, Helaine S, Lewis K, Ackermann M, Aldridge B, Andersson DI, et al. Definitions and guidelines for research on antibiotic persistence. Nature Reviews Microbiology 2019 17:7 [Internet]. 2019 Apr 12 [cited 2023 Aug 29];17(7):441–8. Available from: https://www.nature.com/articles/s41579-019-0196-3

14. Vilchèze C, Hartman T, Weinrick B, Jacobs WR. Mycobacterium tuberculosis is extraordinarily sensitive to killing by a vitamin C-induced Fenton reaction. Nat Commun [Internet]. 2013 [cited 2023 Aug 27];4. Available from: https://pubmed.ncbi.nlm.nih.gov/23695675/

15. Akela AK, Kumar A. Bioenergetic Heterogeneity in Mycobacterium tuberculosis Residing in Different Subcellular Niches. mBio [Internet]. 2021 Jun 1 [cited 2023 Oct 2];12(3). Available from: /pmc/articles/PMC8262966/

16. Schrader SM, Botella H, Jansen R, Ehrt S, Rhee K, Nathan C, et al. Multiform antimicrobial resistance from a metabolic mutation. Sci Adv [Internet]. 2021 Aug 1 [cited 2023 Aug 24];7(35). Available from: https://www.science.org/doi/10.1126/sciadv.abh2037

17. Lobritz MA, Belenky P, Porter CBM, Gutierrez A, Yang JH, Schwarz EG, et al. Antibiotic efficacy is linked to bacterial cellular respiration. Proc Natl Acad Sci U S A [Internet]. 2015 Jul 7 [cited 2023 Aug 16];112(27):8173–80. Available from: https://www.pnas.org/doi/abs/10.1073/pnas.1509743112

18. Patil V, Jain V. Insights into the Physiology and Metabolism of a Mycobacterial Cell in an Energy-Compromised State. J Bacteriol [Internet]. 2019 Oct 1 [cited 2023 Oct 2];201(19). Available from: https://pubmed.ncbi.nlm.nih.gov/31285242/

19. Lu P, Villellas C, Koul A, Andries K, Lill H, Bald D. The ATP synthase inhibitor bedaquiline interferes with small-molecule efflux in Mycobacterium smegmatis. The Journal of Antibiotics 2014 67:12 [Internet]. 2014 Jun 11 [cited 2023 Oct 2];67(12):835–7. Available from: https://www.nature.com/articles/ja201474

20. Jahngen JH, Rossomando EF. Resolution of an ATP-metal chelate from metal-free ATP by reverse-phase high-performance liquid chromatography. Anal Biochem [Internet]. 1983 Apr 15 [cited 2023 Oct 2];130(2):406–15. Available from: https://pubmed.ncbi.nlm.nih.gov/6869828/

21. DISTEFANO V, NEUMAN WF. CALCIUM COMPLEXES OF ADENOSINETRIPHOSPHATE AND ADENOSINEDIPHOSPHATE AND THEIR SIGNIFICANCE IN CALCIFICATION IN VITRO. Journal of Biological Chemistry. 1953 Feb 1;200(2):759–63.

22. Khan MMT, Martell AE. Metal Chelates of Adenosine Triphosphate. Journal of Physical Chemistry (US). 1962 Jan 1;Vol: 66(1):10–5.

23. Tatano Y, Kanehiro Y, Sano C, Shimizu T, Tomioka H. ATP Exhibits Antimicrobial Action by Inhibiting Bacterial Utilization of Ferric Ions. Scientific Reports 2015 5:1 [Internet]. 2015 Feb 25 [cited 2023 Sep 26];5(1):1–8. Available from: https://www.nature.com/articles/srep08610

24. Bhat SA, Iqbal IK, Kumar A. Imaging the NADH: NAD+ homeostasis for understanding the metabolic response of mycobacterium to physiologically relevant stresses. Front Cell Infect Microbiol [Internet]. 2016 Nov 8 [cited 2023 Oct 2];6(NOV):145. Available from: /pmc/articles/PMC5099167/

25. Machová I, Snášel J, Zimmermann M, Laubitz D, Plocinski P, Oehlmann W, et al. Mycobacterium tuberculosis Phosphoenolpyruvate Carboxykinase Is Regulated by Redox Mechanisms and Interaction with Thioredoxin. J Biol Chem [Internet]. 2014 May 5 [cited 2023 Aug 25];289(19):13066. Available from: /pmc/articles/PMC4036320/

26. Borah Slater K, Beyß M, Xu Y, Barber J, Costa C, Newcombe J, et al. One-shot 13 C15 N-metabolic flux analysis for simultaneous quantification of carbon and nitrogen flux. Mol Syst Biol [Internet]. 2023 Mar 9 [cited 2023 Aug 30];19(3). Available from: https://pubmed.ncbi.nlm.nih.gov/36705093/

27. Viljoen AJ, Kirsten CJ, Baker B, Van Helden PD, Wiid IJF. The role of glutamine oxoglutarate aminotransferase and glutamate dehydrogenase in nitrogen metabolism in Mycobacterium bovis BCG. PLoS One. 2013 Dec 19;8(12).

28. Gallant JL, Viljoen AJ, Van Helden PD, Wiid IJF. Glutamate Dehydrogenase Is Required by Mycobacterium bovis BCG for Resistance to Cellular Stress. PLoS One [Internet]. 2016 Jan 1 [cited 2023 Aug 30];11(1). Available from: https://pubmed.ncbi.nlm.nih.gov/26824899/

29. Cao J, Barbosa JM, Singh NK, Locy RD. GABA shunt mediates thermotolerance in Saccharomyces cerevisiae by reducing reactive oxygen production. Yeast [Internet]. 2013 Apr [cited 2023 Aug 30];30(4):129–44. Available from: https://pubmed.ncbi.nlm.nih.gov/23447388/

30. Ramond E, Gesbert G, Rigard M, Dairou J, Dupuis M, Dubail I, et al. Glutamate Utilization Couples Oxidative Stress Defense and the Tricarboxylic Acid Cycle in Francisella Phagosomal Escape. PLoS Pathog [Internet]. 2014 Jan [cited 2023 Aug 30];10(1):e1003893. Available from: https://journals.plos.org/plospathogens/article?id=10.1371/journal.ppat.1003893

31. Jansen RS, Mandyoli L, Hughes R, Wakabayashi S, Pinkham JT, Selbach B, et al. Aspartate aminotransferase Rv3722c governs aspartate-dependent nitrogen metabolism in Mycobacterium tuberculosis. Nature Communications 2020 11:1 [Internet]. 2020 Apr 23 [cited 2023 Aug 25];11(1):1–13. Available from: https://www.nature.com/articles/s41467-020-15876-8

32. Basu P, Sandhu N, Bhatt A, Singh A, Balhana R, Gobe I, et al. The anaplerotic node is essential for the intracellular survival of Mycobacterium tuberculosis. J Biol Chem [Internet]. 2018 Apr 4 [cited 2023 Aug 25];293(15):5695. Available from: /pmc/articles/PMC5900758/

33. Lee JJ, Lee SK, Song N, Nathan TO, Swarts BM, Eum SY, et al. Transient drug-tolerance and permanent drug-resistance rely on the trehalose-catalytic shift in Mycobacterium tuberculosis. Nature Communications 2019 10:1 [Internet]. 2019 Jul 2 [cited 2023 Aug 29];10(1):1–12. Available from: https://www.nature.com/articles/s41467-019-10975-7

34. Nandakumar M, Nathan C, Rhee KY. Isocitrate lyase mediates broad antibiotic tolerance in Mycobacterium tuberculosis. Nature Communications 2014 5:1 [Internet]. 2014 Jun 30 [cited 2023 Aug 25];5(1):1–10. Available from: https://www.nature.com/articles/ncomms5306

35. Mackenzie JS, Lamprecht DA, Asmal R, Adamson JH, Borah K, Beste DJV, et al. Bedaquiline reprograms central metabolism to reveal glycolytic vulnerability in Mycobacterium tuberculosis. Nature Communications 2020 11:1 [Internet]. 2020 Nov 30 [cited 2023 Aug 30];11(1):1–16. Available from: https://www.nature.com/articles/s41467-020-19959-4

36. Zaunbrecher MA, Sikes RD, Metchock B, Shinnick TM, Posey JE. Overexpression of the chromosomally encoded aminoglycoside acetyltransferase eis confers kanamycin resistance in Mycobacterium tuberculosis. Proc Natl Acad Sci U S A [Internet]. 2009 Nov 24 [cited 2023 Aug 29];106(47):20004–9. Available from: https://pubmed.ncbi.nlm.nih.gov/19906990/

37. Vilchèze C, Hartman T, Weinrick B, Jain P, Weisbrod TR, Leung LW, et al. Enhanced respiration prevents drug tolerance and drug resistance in Mycobacterium tuberculosis. Proc Natl Acad Sci U S A [Internet]. 2017 Apr 25 [cited 2023 Aug 27];114(17):4495–500. Available from: https://pubmed.ncbi.nlm.nih.gov/28396391/

38. Grant SS, Kaufmann BB, Chand NS, Haseley N, Hung DT. Eradication of bacterial persisters with antibiotic-generated hydroxyl radicals. Proc Natl Acad Sci U S A [Internet]. 2012 Jul 24 [cited 2023 Aug 27];109(30):12147–52. Available from: https://www.pnas.org/doi/abs/10.1073/pnas.1203735109

39. Rowe SE, Wagner NJ, Li L, Beam JE, Wilkinson AD, Radlinski LC, et al. Reactive oxygen species induce antibiotic tolerance during systemic Staphylococcus aureus infection. Nat Microbiol [Internet]. 2020 Feb 1 [cited 2023 Aug 16];5(2):282–90. Available from: https://pubmed.ncbi.nlm.nih.gov/31819212/

40. Mishra R, Kohli S, Malhotra N, Bandyopadhyay P, Mehta M, Munshi MH, et al. Targeting redox heterogeneity to counteract drug tolerance in replicating Mycobacterium tuberculosis. Sci Transl Med [Internet]. 2019 Nov 13 [cited 2023 Aug 24];11(518). Available from: https://pubmed.ncbi.nlm.nih.gov/31723039/

41. Lobritz MA, Andrews IW, Braff D, Porter CBM, Gutierrez A, Furuta Y, et al. Increased energy demand from anabolic-catabolic processes drives β-lactam antibiotic lethality. Cell Chem Biol [Internet]. 2022 Feb 17 [cited 2023 Aug 27];29(2):276-286.e4. Available from: https://pubmed.ncbi.nlm.nih.gov/34990601/

42. Yang JH, Wright SN, Hamblin M, McCloskey D, Alcantar MA, Schrübbers L, et al. A White-Box Machine Learning Approach for Revealing Antibiotic Mechanisms of Action. Cell [Internet]. 2019 May 30 [cited 2023 Aug 27];177(6):1649-1661.e9. Available from: https://pubmed.ncbi.nlm.nih.gov/31080069/

43. Lee AJ, Wang S, Meredith HR, Zhuang B, Dai Z, You L. Robust, linear correlations between growth rates and β-lactam-mediated lysis rates. Proc Natl Acad Sci U S A [Internet]. 2018 Apr 17 [cited 2023 Aug 27];115(16):4069–74. Available from: https://www.pnas.org/doi/abs/10.1073/pnas.1719504115

44. Greulich P, Scott M, Evans MR, Allen RJ. Growth-dependent bacterial susceptibility to ribosome-targeting antibiotics. Mol Syst Biol [Internet]. 2015 Mar 1 [cited 2023 Aug

27];11(3):796. Available from: https://onlinelibrary.wiley.com/doi/full/10.15252/msb.20145949

45. Haugan MS, Løbner-Olesen A, Frimodt-Møller N. Comparative activity of ceftriaxone, ciprofloxacin, and gentamicin as a function of bacterial growth rate probed by Escherichia coli chromosome replication in the mouse peritonitis model. Antimicrob Agents Chemother [Internet]. 2019 Feb 1 [cited 2023 Aug 27];63(2). Available from: https://journals.asm.org/doi/10.1128/aac.02133-18

46. Lopatkin AJ, Stokes JM, Zheng EJ, Yang JH, Takahashi MK, You L, et al. Bacterial metabolic state more accurately predicts antibiotic lethality than growth rate. Nature Microbiology 2019 4:12 [Internet]. 2019 Aug 26 [cited 2023 Aug 27];4(12):2109–17. Available from: https://www.nature.com/articles/s41564-019-0536-0

47. Conlon BP, Rowe SE, Gandt AB, Nuxoll AS, Donegan NP, Zalis EA, et al. Persister formation in Staphylococcus aureus is associated with ATP depletion. Nat Microbiol [Internet]. 2016 Apr 18 [cited 2023 Aug 28];1(5). Available from: /pmc/articles/PMC4932909/

48. Shan Y, Gandt AB, Rowe SE, Deisinger JP, Conlon BP, Lewis K. ATP-Dependent Persister Formation in Escherichia coli. mBio [Internet]. 2017 Jan 1 [cited 2023 Aug 28];8(1). Available from: https://pubmed.ncbi.nlm.nih.gov/28174313/

49. Peng B, Su YB, Tian YM, Correspondence XXP. Exogenous Alanine and/or Glucose plus Kanamycin Kills Antibiotic-Resistant Bacteria. 2015 [cited 2023 Aug 28]; Available from: http://dx.doi.org/10.1016/j.cmet.2015.01.008

50. Shetty A, Dick T. Mycobacterial Cell Wall Synthesis Inhibitors Cause Lethal ATP Burst. Front Microbiol [Internet]. 2018 Aug 15 [cited 2023 Aug 28];9(AUG). Available from: https://pubmed.ncbi.nlm.nih.gov/30158918/

51. Lee BS, Kalia NP, Jin XEF, Hasenoehrl EJ, Berney M, Pethe K. Inhibitors of energy metabolism interfere with antibiotic-induced death in mycobacteria. J Biol Chem [Internet]. 2019 Feb 2 [cited 2023 Aug 28];294(6):1936. Available from: /pmc/articles/PMC6369303/

52. Ojha AK, Baughn AD, Sambandan D, Hsu T, Trivelli X, Guerardel Y, et al. Growth of Mycobacterium tuberculosis biofilms containing free mycolic acids and harbouring drug-tolerant bacteria. Mol Microbiol [Internet]. 2008 Jul [cited 2023 Aug 29];69(1):164–74. Available from: https://pubmed.ncbi.nlm.nih.gov/18466296/

53. Samuels AN, Wang ER, Harrison GA, Valenta JC, Stallings CL. Understanding the contribution of metabolism to Mycobacterium tuberculosis drug tolerance. Front Cell Infect Microbiol. 2022 Aug 22;12:958555.

54. Lobritz MA, Belenky P, Porter CBM, Gutierrez A, Yang JH, Schwarz EG, et al. Antibiotic efficacy is linked to bacterial cellular respiration. Proc Natl Acad Sci U S A [Internet]. 2015 Jul 7 [cited 2023 Oct 2];112(27):8173–80. Available from: https://www.pnas.org/doi/abs/10.1073/pnas.1509743112

55. Formation Constants and Heat Stability of Calcium and Magnesium - PDF Free Download [Internet]. [cited 2023 Sep 26]. Available from: https://datapdf.com/formation-constants-and-heat-stability-of-calcium-and-magnes.html

56. Kitzenberg DA, Lee JS, Mills KB, Kim JS, Liu L, Vázquez-Torres A, et al. Adenosine Awakens Metabolism to Enhance Growth-Independent Killing of Tolerant and Persister Bacteria across Multiple Classes of Antibiotics. mBio [Internet]. 2022 Jun 1 [cited 2023 Aug 27];13(3). Available from: https://journals.asm.org/doi/10.1128/mbio.00480-22

57. Baquero F, Levin BR. Proximate and ultimate causes of the bactericidal action of antibiotics. Nature Reviews Microbiology 2020 19:2 [Internet]. 2020 Oct 6 [cited 2023 Aug 29];19(2):123–32. Available from: https://www.nature.com/articles/s41579-020-00443-1

58. Edna George 1 AG 1, TL 2, PP 1, SI 1, IG 1, LS 1, SJ 1, PRS 1, AAD 1, RM 2, RA. Immunomodulatory effect of mycobacterial outer membrane vesicles coated nanoparticles. Biomaterial Advances.

59. Cox J, Mann M. MaxQuant enables high peptide identification rates, individualized p.p.b.-range mass accuracies and proteome-wide protein quantification. Nature Biotechnology 2008 26:12 [Internet]. 2008 Nov 30 [cited 2023 Aug 30];26(12):1367–72. Available from: https://www.nature.com/articles/nbt.1511

60. Tyanova S, Temu T, Cox J. The MaxQuant computational platform for mass spectrometry-based shotgun proteomics. Nature Protocols 2016 11:12 [Internet]. 2016 Oct 27 [cited 2023 Aug 30];11(12):2301–19. Available from: https://www.nature.com/articles/nprot.2016.136

61. Cox J. Accurate proteome-wide label-free quantification by delayed normalization and maximal peptide ratio extraction, termed MaxLFQ. Mol Cell Proteomics. 2014;13:2513–26.

62. Tyanova S, Temu T, Sinitcyn P, Carlson A, Hein MY, Geiger T, et al. The Perseus computational platform for comprehensive analysis of (prote)omics data. Nature Methods 2016 13:9 [Internet]. 2016 Jun 27 [cited 2023 Aug 30];13(9):731–40. Available from: https://www.nature.com/articles/nmeth.3901

63. Bindea G, Mlecnik B, Hackl H, Charoentong P, Tosolini M, Kirilovsky A, et al. ClueGO: a Cytoscape plug-in to decipher functionally grouped gene ontology and pathway annotation networks. Bioinformatics [Internet]. 2009 Apr 4 [cited 2023 Aug 30];25(8):1091. Available from: /pmc/articles/PMC2666812/

64. Gengenbacher M, Rao SPS, Pethe K, Dick T. Nutrient-starved, non-replicating Mycobacterium tuberculosis requires respiration, ATP synthase and isocitrate lyase for maintenance of ATP homeostasis and viability. [cited 2023 Sep 3]; Available from: http://mic.sgmjournals.org

65. Thomson M, Liu Y, Nunta K, Cheyne A, Fernandes N, Williams R, et al. Expression of a novel mycobacterial phosphodiesterase successfully lowers cAMP levels resulting in reduced tolerance to cell wall–targeting antimicrobials. Journal of Biological Chemistry [Internet]. 2022 Aug 1 [cited 2023 Aug 23];298(8). Available from: http://www.jbc.org/article/S0021925822005932/fulltext